RSC Advances

REVIEW

View Article Online
View Journal | View Issue

Cite this: *RSC Adv.*, 2023, **13**, 4678

Adsorptive removal of antibiotic pollutants from wastewater using biomass/biochar-based adsorbents

Oluwaseyi Aderemi AJALA, [a] Solomon Oluwaseun AKINNAWO, †[bc] Abayomi BAMISAYE, †[d] Demilade Tunrayo ADEDIPE, †[e] Morenike Oluwabunmi ADESINA,†[d] Omolabake Abiodun OKON-AKAN,†[bf] Tosin Adewumi ADEBUSUYI, †[g] Adedamola Titi OJEDOKUN,†[b] Kayode Adesina ADEGOKE *[b] and Olugbenga Solomon BELLO *[b]

Received 12th October 2022
Accepted 22nd December 2022

DOI: 10.1039/d2ra06436g

rsc.li/rsc-advances

This study explores adsorptive removal measures to shed light on current water treatment innovations for kinetic/isotherm models and their applications to antibiotic pollutants using a broad range of biomass-based adsorbents. The structure, classifications, sources, distribution, and different techniques for the remediation of antibiotics are discussed. Unlike previous studies, a wide range of adsorbents are covered and adsorption of comprehensive classes of antibiotics onto biomass/biochar-based adsorbents are categorized as β-lactam, fluoroquinolone, sulfonamide, tetracycline, macrolides, chloramphenicol, antiseptic additives, glycosamides, reductase inhibitors, and multiple antibiotic systems. This allows for an

[a]*Department of Applied Chemistry, Graduate School of Advanced Science and Engineering, Hiroshima University, 1-4-1, Kagamiyama, Higashi-Hiroshima, 739-8527, Japan*

[b]*Department of Pure and Applied Chemistry, Ladoke Akintola University of Technology, P. M. B. 4000, Ogbomoso, Oyo State, Nigeria*

[c]*Department of Chemical Sciences, Olusegun Agagu University of Science and Technology, P. M. B. 353, Okitipupa, Ondo State, Nigeria*

[d]*Department of Chemical Sciences, Faculty of Natural and Applied Sciences, Lead City University, Ibadan, Oyo State, Nigeria*

[e]*State Key Laboratory of Marine Pollution and Department of Chemistry, City University of Hong Kong, Tat Chee Avenue, Kowloon, Hong Kong SAR, China*

[f]*Wood and Paper Technology Department, Federal College of Forestry Jericho, Ibadan, Nigeria*

[g]*Department of Chemical Sciences, Augustine University, Ilara-Epe, Lagos State, Nigeria. E-mail: kwharyourday@gmail.com; osbello@lautech.edu.ng*

† Share the same second authorship.

Olugbenga Solomon Bello is a Professor of Physical Chemistry in the Department of Pure and Applied Chemistry, Ladoke Akintola University of Technology, Ogbomoso, Oyo State, Nigeria. He completed his PhD in Physical Chemistry at the University of Ibadan, Nigeria in 2008. He was the recipient of the 2019 Nigerian Academy of Science Gold Medal Award in Physical Sciences. He received the African Union-Third World Academy of Science (AU-TWAS) Young Scientists National Award in 2012 and the Prof. Kayode Adebowale Young Scientist Prize in Chemical Sciences organized by Nigerian Young Academy in 2016. He benefited from the USM-TWAS Postdoctoral and Visiting Scholar Fellowships to the School of Chemical Engineering University of Science Malaysia. He won TWAS research grant (2012 and 2015) and Tertiary Education Trust Fund (TETFUND) Institutional Based Research (IBR) in 2016. He was nominated and recognized as one of the "175 Faces of Chemistry" worldwide by the Royal Society of Chemistry, UK. He was listed among the 2% most cited Scientists in the world by a group of Stanford University researchers. His research interest is focused on adsorption of heavy metals, dyes and pharmaceuticals from wastewaters using agricultural waste materials as adsorbents in lieu of expensive commercial activated carbon to bio-remediate the environment. His accomplishment, as well as the significant impact of his research findings has contributed immensely to environmental protection and conservation. It has positively impacted stakeholders like environmentalists, water purification experts and those in the medical disciplines. He has mentored several postgraduate students and published over one hundred articles in high impact national and international journals. He has delivered keynote and lead papers at national and international conferences. He has served as external examiners and assessors to many universities at national and international levels. He has served on various committees as chairman and members at the departmental, faculty and university levels. He is the Managing Editor of Science Focus Journal published by the Faculty of Pure and Applied Sciences, LAUTECH, Ogbomoso.

assessment of their performance and an understanding of current research breakthroughs in applying various adsorbent materials for antibiotic removal. Distinct from other studies in the field, the theoretical basis of different isotherm and kinetics models and the corresponding experimental insights into their applications to antibiotics are discussed extensively, thereby identifying the associated strengths, limitations, and efficacy of kinetics and isotherms for describing the performances of the adsorbents. In addition, we explore the regeneration of adsorbents and the potential applications of the adsorbents in engineering. Lastly, scholars will be able to grasp the present resources employed and the future necessities for antibiotic wastewater remediation.

1 Introduction

Through the years, lives have been saved thanks to the discovery of antibiotics and their application in treating diseases, notably bacterial infections.[1] Researchers are searching for more antibacterial chemical compounds, but they are constrained by the possibility of negative side effects. Due to an increase in the world population, there is a rise in the use of antibiotics, necessitating the development of better medications, apart from their use for non-medical purposes, which is a major contribution to their consumption.[2] Since antibiotics are not completely digested after consumption, they can be discovered in sewage systems.[3] These non-digested antibiotics are frequently not biodegradable and photolysis is useless against them. According to a recent study, India has been the world's most substantial end-user since 2015, posing a serious threat to their resistance.[4–8] Antibiotics can be detected in water samples due to ineffective conventional methods of elimination from wastewater.[9,10] However, some metabolized antibiotics are eliminated through defecation while the active non-biodegradable residues accumulate greatly, developing bacteria with antibiotic-resistance.[11] As a result, antibiotic-resistant germs kill thousands of people yearly worldwide.[12] Antimicrobial resistance reported in detectable concentrations in drinkable water is lower than that found in numerous effluents, such as hospital discharges, pharmaceutical industry emissions, and agricultural water.[5,10,13] Antibiotic levels in the environment are also exacerbated by pharmaceutical firms and ineffective industrial wastewater treatment. According to the current literature, tetracyclines, sulfonamides, quinolones, ionophores, and lactams are quickly adsorbed but difficult to disintegrate.[14] Conventional treatment plants only treated 48–77%,[15] despite the fact that the presence of antibiotics in drinking water precedes the increase in antibiotic-resistant bacteria and transmission to both human and animal pathogens, posing serious hygienic and quantifiable clinical risks. Although existing treatment technologies cannot totally eliminate the problem, addressing the problem at its source can help prevent additional contamination of ecosystems. Because of their great variety and complete classification, separating antibiotics from wastewater necessitates the use of special procedures.

Wide-ranging experimental reports on antibiotic adsorption and numerous studies on the kinetic and isotherm models have been reported. However, a review of these models is absent, thereby necessitating an extensive study in these areas, focusing on the adsorption technique. In addition, the previous literature did not cover the extensive utilization of biomass/biochar-based adsorbents for the removal of comprehensive classes of antibiotics. Additionally, the potential applications of adsorbents in engineering included in this study were not mentioned in past studies. As a result, our research is limited to the adsorptive removal of antibiotics utilizing various adsorbents. Unlike the previous literature, broad ranges of adsorbents are covered. They are categorized into the adsorption of different classes of antibiotics, including β-lactam, fluoroquinolone, sulfonamide, tetracycline, macrolides, chloramphenicol, antiseptic additives, glycosamides, reductase inhibitors, and multiple antibiotics systems onto agricultural biomass/biochar-based adsorbents. This provides an opportunity to assess their performances and understand current research breakthroughs in applying various adsorbent materials for the removal of antibiotics, thereby identifying the associated strengths and limitations and experimental insights into the efficacy of different kinetics and isotherms for describing the performances of the adsorbents. Regeneration of adsorbents and the potential applications of the adsorbents in engineering are also explored. Lastly, this study highlights significant challenges and knowledge gaps for directing specific research for large and industrial-scale applications.

2 Antibiotic: structure, classifications, sources, and distribution

Antibiotics are divided into two major groups according to their mode of operation: bacteriostatic (restrains bacterial progression) and bactericidal (kills bacteria). The classification of antibiotics based on their structural unit is presented in (Table 1), along with some frequent sources (Fig. 1). Antibiotic concentrations can be detected from many sources to compile data for further research into antibiotic remediation worldwide. Ciprofloxacin (CPX) was abundantly prevalent in wastewater, followed by sulfamethoxazole.[16] Quinolones are categorized as non-decomposable.[16] Liquid chromatography combined with mass spectrometry (LC-MS/MS) and solid-phase extraction (SPE) are commonly used to extract antibiotics.[17,18] Antibiotics in groundwater have been identified in surface water and effluents from hospitals, such as erythromycin, amoxicillin, norfloxacin, ciprofloxacin, levofloxacin, ofloxacin, trimethoprim, sulfamethoxazole, and tetracycline, as well as other medications in the g L^{-1} range. Sources of antibiotics have a direct impact on bacterial resistance. Hospital and untreated household discharge, which flows straight into the sewage system, are substantial contributors (Fig. 1).

Table 1 Examples of different classes of antibiotics and their chemical structures

Class	Structure	Example	Side effects/toxicity level
β-Lactams	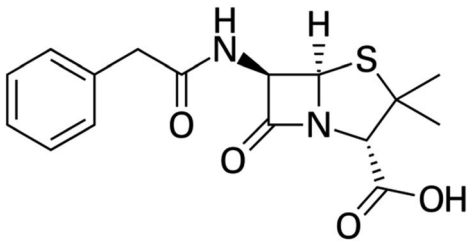	Phenoxy penicillin	Inhibition of cell wall synthesis
	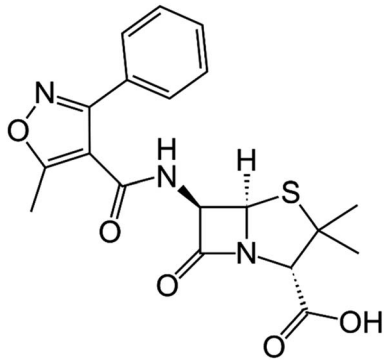	Oxacillin	Inhibition of cell wall synthesis
	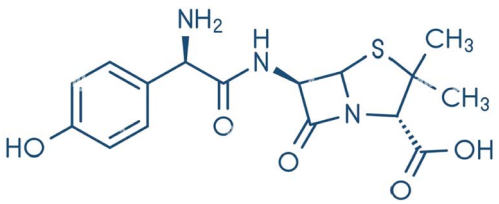	Amoxicillin	Inhibition of cell wall synthesis
	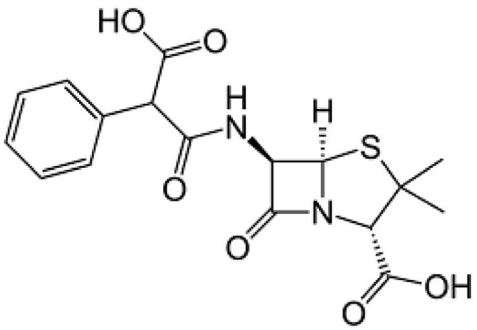	Carbenicillin	Inhibition of cell wall synthesis
	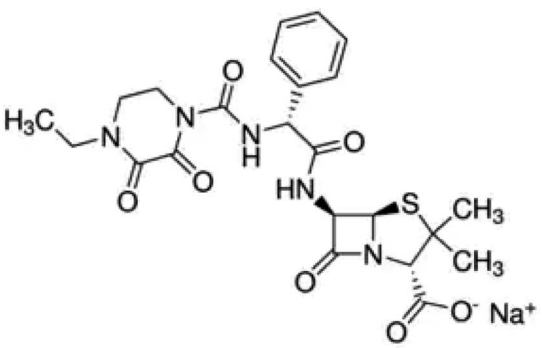	Piperacillin	Inhibition of cell wall synthesis

Table 1 (*Contd.*)

Class	Structure	Example	Side effects/toxicity level
Tetracyclines	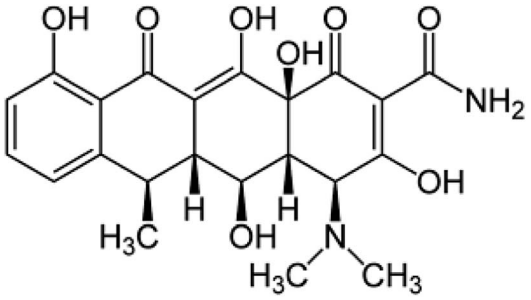	Doxycycline	Inhibition of protein synthesis
Aminoglycosides	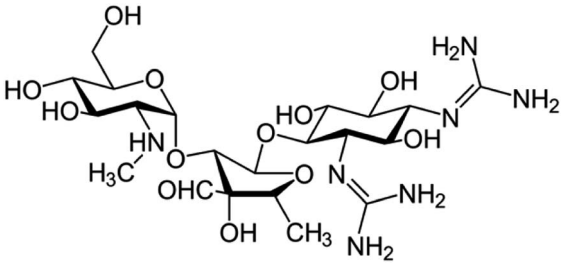	Gentamicin 1c	Inhibition of protein synthesis
Macrolides	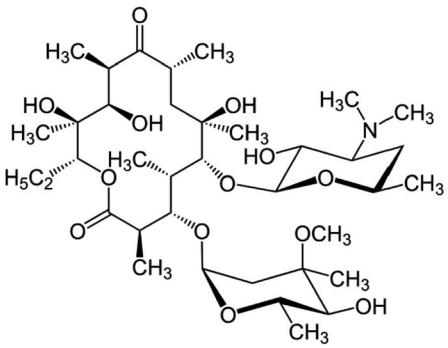	Erythromycin A	Inhibition of protein synthesis
Glycopeptides	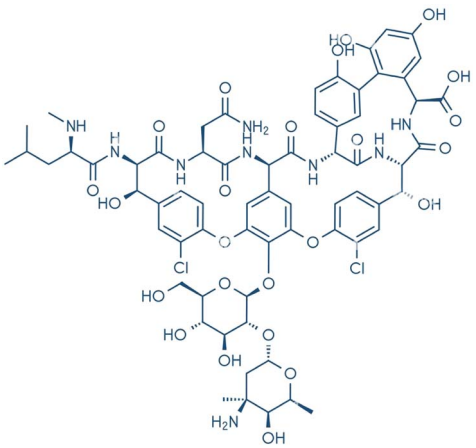	Vancomycin	Inhibition of nucleic acids synthesis
Sulfonamides	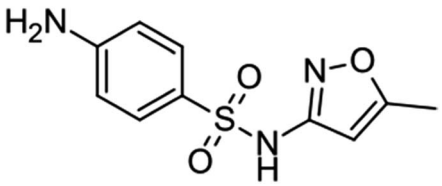	Sulfamethoxazole	Blockage of folic acid metabolism

Table 1 (*Contd.*)

Class	Structure	Example	Side effects/toxicity level
Quinolones	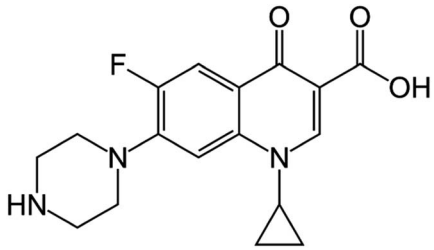	Ciprofloxacin	Inhibition of nucleic acid synthesis

Fig. 1 Common sources and distributions of antibiotics in the environment.[30–33]

Table 2 Different techniques for antibiotics remediation, including their advantages and disadvantages

Method	Advantages	Disadvantages	Examples of antibiotics removed
Adsorption	It is easy to operate and has low cost	Product recovery usually requires expensive distillation. The capacity of the adsorbent also progressively deteriorates as you increase the number of cycles	Chlortetracycline,[51] sulfamethazine[52]
Photolysis and photocatalysis	It does not lead to the formation of bromated products. It can be applied to the full-scale drinking water treatment system	The penetration of light can be inhibited by turbidity. The process is also energy- and cost-intensive	Tetracycline,[53] ciprofloxacin[54]
Ozonation	It enhances the effective destruction of organic matter	It requires high cost	Roxithromycin[55]
Biodegradation	It is a low-cost technology and plays a critical role in pollutant degradation	The rate of microbial metabolism may reduce (due to antibiotic wastewater exposure), thereby affecting the performance of biological treatment of the sewage	Cephalexin,[41] sulfanilamide[56]
Electrochemical oxidation	It can be integrated with other technologies	It is not widely used due to the expensive cost of electrode materials. It is also associated with low current efficiency and high energy consumption	Levofloxacin[57]
Anaerobic treatment	It is effective in removing high-strength organic compounds and breaking down refractory materials	They are effective in removing non-organic pollutants from wastewater (such as nutrients and pathogens)	Tylosin,[58] penicillin[59]
Aerobic treatment	It is associated with reduced odor and improved nutrient removal efficiency	It requires high capital cost, high operating cost, and high maintenance requirements	Tetracycline,[60] Sulfamerazine[46]
Biofilm technology	It offers operational flexibility, reduced hydraulic retention time, low space requirements, high active biomass concentration, and increased biomass residence time	Operators need to be skilled in the area of biological water treatment. It also requires annual monitoring to ensure that the bacteria on the carriers are still thriving	Ibuprofen,[61] terramycin[62]
Coagulation/flocculation/sedimentation	Decrease in detention time of the wastewater treatment process. They can also target different contaminants *via* a single system	Since coagulation is an additive process, the addition of chemicals can produce a large volume of sludge that must be treated and disposed of after the treatment	Sulfamerazine, sulfadimethoxine[48]

Antibiotics and associated genes have recently been discovered in water samples all around the world due to their limited biodegradability, which can have a significant influence on human and animal health. Non-target infections are affected by antibiotics in aqueous media, and the algal structure is altered.[19] The existence of antibiotics in groundwater, surface water, and wastewater, even at minimal amounts, is a serious problem, and numerous strategies for antibiotic removal from effluents have been implemented. Countless traditional procedures, such as distillation, reverse osmosis, sedimentation, and lime softening, are used at different phases of wastewater treatment; however, despite their low cost and harmless nature, these technologies are ineffective in entirely eliminating them from wastewater.[20–22]

Regardless of the use of foremost and derived wastewater treatments, external particles such as medicines, heavy metal ions and dyes continue to be released, which contain dangerous residues of hazardous pollutants. As a result, advanced treatment is required to eradicate dangerous contaminants.[14] Effluent treatment using a technique other than traditional methods was investigated by De Andrade and his co-authors, including flotation, lime softening and coagulation, and innovative types of expertise such as advanced oxidation and ozonation, membrane separation, and electrodialysis because these processes require fewer chemicals.[23] Nevertheless, when interacting with Cl_2 or O_3, some of these procedures produce poisonous by-products that are considerably more dangerous than the initial pollutants. As a result, these technologies are not in use because of their high energy requirements and inability to remediate wastewater on a larger scale attributed to their expensive cost. Reverse osmosis and nanofiltration have recently been focused on based on their high energy and material consumption.[7,24] Conversely, these technologies exhibit several drawbacks, such as the waste of too much water in reverse osmosis/nanofiltration. In addition, the method is time-consuming and expensive to implement on a large scale.[25]

Furthermore, innovative hybrid-designed biological systems for wastewater treatment that combine various redox conditions and biomass conformations may successfully remove various antibiotic chemicals. However, further in-depth research is needed to assess their efficacy in full-scale wastewater treatment plants with a variety of operating characteristics. Currently, adsorption has various advantages over alternative remediation approaches, including simplicity, reliability, minimal energy use, and quick adsorbent recovery.[26] The batch process and the continuous process are the major adsorptive processes for the removal of antibiotics from wastewater, both of which can be used with a variety of adsorbents, such as biochars, clay materials, ion-exchange resins, activated carbons (ACs), zeolites and carbon nanotubes (CNT). Because this technique has various improvements compared to other procedures, and because it is simple to combine with other technologies, incorporating a unified system into previously existing treatment plants for total elimination could be helpful. Several hybrid systems previously created by combining membrane technologies with other efficient technologies include ozonolysis, photocatalysis, chlorination, sedimentation, and filtration.[27–29] However, these pairings possess some drawbacks, *e.g.*, the aerobic digestion process frequently generates more damaging derivatives than the organic molecules themselves. Table 2 shows numerous treatment techniques for removing various antibiotics discovered thus far. Adsorbents such as CNTs, clay materials, ACs (PAC/GAC), and biochar have also been comprehensively researched for antibiotic elimination.[25]

3 Different techniques for antibiotics remediation

Antibiotics and adsorption are closely related.[34] Adsorption and activated carbon (AC) have a close association, showing that AC is the most studied adsorbent. This is due to activated carbon's low cost and its well-developed pore structure and abundance of surface functional groups, which allow for both physical and chemical adsorption of antibiotics. Adsorption efficiency is affected by the kind of activated carbon, operating parameters (pH, adsorbent dosage, and ionic strength), activation methods, precursors, and adsorbates, used in the process.[35] For instance, the size of granular activated carbon particles has a major impact on removing certain pollutants, with the smallest sizes exhibiting maximum removal effectiveness, which is likely to be due to greater mass transfer.[36,37] Activated carbon can be modified in a variety of ways to boost its adsorption capacity by modifying the pore structure and surface chemical properties.

After adsorption, photolysis/photocatalysis is the most researched therapeutic method. Despite the fact that both photolysis and photocatalysis involve light, their methods are somewhat different. Self-sensitization, and indirect and direct photolysis are the three photolysis routes. After photon adsorption, chemicals undergo pyrolysis, heterolysis, and photoionization. Indirect photolysis is induced by compounds found in the environment which absorb light energy and destroy organic matter by producing highly reactive molecules, including alkyl peroxy radicals (OOR), hydroxyl radicals (·HO), and singlet oxygen ($^1O_2$). Organics transition to an excited state by collecting light energy, transferring it to ground-state $^3O_2$ or H_2O, and releasing reactive oxygen species like O_2 and ·OH, which destroy the organics' ground-state molecules.[38]

Photocatalysis has been getting a lot of attention lately. Its high mineralization efficiency for refractory organic contaminants makes it one of the most sophisticated oxidation processes. However, TiO_2 only reacts to UV light. Additionally, g-C_3N_4 (and other newly developed visible-light-response catalysts) have a low quantum yield. As a result, there is still a long way to go in terms of the large-scale deployment of these photocatalysts.

Ozonation, like photocatalysis, is an advanced oxidation process with direct ozone oxidation and indirect ozone oxidation by ·OH as mechanisms. Due to the increase in reactive radicals (·OH) and the presence of indirect reactions, alkaline ozonation results in high chemical oxygen demand and total organic carbon removal rates. In contrast, the reaction is dominated by direct oxidation under acidic conditions and has a limited ability to remove pollutants.[39]

Apart from being an important route for breaking antibiotics down in the environment, biodegradation is also one of the most widely employed techniques for treating sewage in antibiotic wastewater. Biodegradation research hotspots are the conditions, consequences, and mechanisms.[40] The most often utilized method is activated sludge. The efficiency of this method is largely determined by the adsorption and biodegradation capabilities of the sludge. Adsorption process is used to remove antibiotics like norfloxacin, ciprofloxacin, ofloxacin, ampicillin, β-lactams, quinolones, and tetracyclines, whereas biodegradation is used to remove antibiotics like cephalexin and β-lactams.[41]

Conventional activated sludge treatment technologies are unable to extract sulfonamide antibiotics fully. However, because of the exposure to antibiotic wastewater, the rate of microbial metabolism may reduce, thereby affecting the performance of biological treatment of the sewage. The use of technologies such as ozonation to pre-treat antibiotic effluent is an excellent technique to lessen the biological unit's disposal difficulties.

Electrochemical oxidation has grown in popularity as a therapeutic method. To a large extent, the electrochemical oxidation ability and efficiency are determined by the electrode materials' catalytic activity and stability, particularly the anode electrode.[42] Electrode materials widely employed in electrochemical oxidation include platinum electrodes, dimensionally stable anodes, and boron-doped diamond electrodes. However, due to the expensive cost of electrode materials, electrochemical oxidation has not been widely utilized. Furthermore, when the conductivity of wastewater is low, mass transfer in the electrochemical oxidation reactor is slow, leading to a low current efficiency and high energy consumption. As a result, low-cost anode materials that have high stability and catalytic activity are needed. Additionally, new reactors, like the three-dimensional electrode reactor, should be studied to reduce mass transfer resistance and enhance current efficiency for electrochemical oxidation technology to be widely used.

Hydrolysis, acidogenesis, and methanogenesis are all steps in the anaerobic treatment process. Extracellular enzymes degrade solid cellulose, lignins, lipids, proteins, and complex organics into soluble organic fatty acids, carbon dioxide, ammonia, and alcohol in the hydrolysis phase, while microorganisms convert the products of the first stage into acetic acid, hydrogen, carbon dioxide, propionic acid, and other low molecular weight organic acids in the acidogenesis phase. Two groups of methane-forming bacteria work simultaneously in the final stage, the methanogenesis phase, to convert carbon dioxide and hydrogen to methane, while converting acetate to bicarbonate and methane.

For aerobic treatment, organic substances can be entirely degraded to CO_2 in an aerobic process.[43,44] Anaerobic processes have been used more frequently for antimicrobial wastewater treatment than aerobic processes. Nonetheless, certain antibiotics can be entirely metabolized to carbon dioxide and water under aerobic circumstances. The aerobic procedure would not be practicable for high-strength effluent from antibiotics manufacturers; hence, before aerobic treatment, dilution of the wastewater is required. As a result, the micro-aerobic or integrated anaerobic–aerobic process is capable of treating high-strength antibiotic manufacturing wastewater.[45,46] COD has been employed to indicate process performance in most of the research mentioned above. However, it should be noted that high efficiency in removing COD does not imply high efficiency in removing antibiotics. As a result, direct detection of antibiotic concentration rather than using COD is strongly advised in future research.

Microorganisms used in biological processes typically come in two forms: biofilms and suspended activated sludge. Biofilms are microorganism aggregates that grow on a solid packaging substance. They have previously been identified as highly complex, diverse, and uncontrolled formations. The thickness and form of biofilm seen are a product of the operating parameters of the biofilm system.[47] Biofilms are clusters with a mushroom-like appearance and cavities. Voids are open passages that connect the bulk fluid to the interior of biofilms. The liquid may flow through the spaces but is always stationary in the cell clusters. As a result, both convection and diffusion in voids may contribute to mass transfer, whereas only diffusion determines transport in cell clusters. Knowledge of the biofilms used in the treatment of wastewater polluted with antibiotics is currently limited.

Coagulation/flocculation/sedimentation is a method of removing soluble species in which chemicals are applied to water to promote colloidal particle instability, permitting aggregation through flocculation and then sedimentation. In this method, antibiotics would be brought into contact with clays and other natural colloidal matter for long periods in a natural system, affording the chance for antibiotic adsorption on the colloidal matter. If antibiotics are adsorbed on colloids, they could be co-removed in the coagulation, flocculation, and sedimentation process. On the other hand, Adams *et al.*[48] found no substantial remediation of the antibiotics examined using ferric salt or aluminium as a coagulant. This method of removing antibiotics is not yet proven.

Despite the advantages of some available methods (Table 2), they have disadvantages, including poor removal efficiency, high energy requirements, production of poisonous by-products, which may pose health risks, and the production of large quantities of secondary sludge, that are harmful to both aquatic and human health.[7] The adsorption technique using activated carbon (AC), has gained increasing attention due to its lower cost, simplicity of operation, large surface area, and efficacy.[7] By comparison, adsorption is still the most prevalent method of treating wastewater for the two types of antibiotics because of the advantages of ease of operation and low cost. Carbon materials, like graphene oxide, biochar, activated carbon, and nanocarbon materials, like nanoporous carbon and nanotubes, can be used as adsorbents for antibiotics removal;[49] other materials include chitosan beads, and bentonite.[50]

4 Agricultural biomass-based adsorbents for antibiotics removal

In recent years, the search for a simple, green, effective, inexpensive and sustainable material to control antibiotics has led

the scientific community to develop a significant interest in a non-toxic and readily available agricultural biomass material for the adsorptive removal of antibiotic contaminants in water and wastewater.[63] Agricultural biomass is a group of residues obtained from either forestry or agricultural undertakings (Table 3). Biomass-based adsorbents obtained from agricultural residues have been suggested to retain functional groups that include hydroxyl and carboxyl groups that expedite the removal of emerging contaminants that include pharmaceuticals such as antibiotics. Biochar and activated carbon obtained from agricultural biomass have been widely explored for the removal of pollutants in the water phase.

Biochar is a carbon-rich product of biomass pyrolysis in an inert atmosphere (Table 3). The growing interest in biochar over the years for the adsorption of aqueous pollutants is owing to its intrinsic properties, such as its high specific surface areas and porous structure, surface functionality, and vast possibilities for modification.[64] Its properties are mainly dependent on heating temperature, biomass type, carrier gases and catalysts.[33]

Due to advances in research, diverse methods have been devised to influence the properties of biochar depending on the method of preparation and modification so that they unveil a better adsorption capacity.[33,65] Bare biochars can be obtained *via* physical methods (ball milling and microwave pyrolysis) or chemical methods using oxidants such as HCl, H_2SO_4, H_3PO_4, or reductants NaOH, KOH during pre- or post-synthesis. Some pristine or bare biochars are usually associated with a lack of affinity for antibiotic pollutants, which is influenced by the absence of sufficient surface functionality or their low porosity as an adsorbent, so they are subjected to modifications. Modified biochars using the aforementioned activating agents are referred to as activated carbon (AC).

AC is carbon produced from carbonaceous source materials mainly from biomass, *e.g.* coconut husk or wood, purportedly exhibiting large pore volumes, a well-built high specific area, small pore diameter, and high adsorption capacity and have been projected as one of the most effectual adsorbents (Table 3). Nevertheless, the characteristics of the prepared activated carbon depend on the raw precursors utilized and the preparation procedure, as depicted in Fig. 2.[66,67] They have been found to have relatively comparable adsorption properties to commercial activated carbon. Additionally, they are more cost effective than commercial activated carbon. Furthermore, apart from modifying bare biochar using various activating agents, combining them with other components, such as clay minerals, graphene, metal oxides or hydroxides, graphene oxides, carbon nanotubes and polymers to form composites, has been employed to enhance their antibiotic removal efficiency. Biochar can be incorporated with these components either before pyrolysis or after pyrolysis.

However, it is vital to select adsorbents with higher selectivity for targeted antibiotics because it is often challenging to control the type of contaminant occurring in a matrix or adsorption variables such as pH and temperature.[63,68] The process of adsorbing contaminant molecules onto biomass-based adsorbents has been found to follow the principal steps of adsorption, which include: the movement of adsorbate molecules from the matrix, diffusion of the adsorbate through the liquid film surrounding the adsorbent molecule, movement of adsorbate molecules to the active sites of the adsorbent and adsorbent–adsorbent interactions, while the mechanism of adsorption depends on the latter step.[33,69]

Different interaction types have been postulated to be responsible for antibiotics adhering to the surface of biochar or (AC): for example, electrostatic, hydrophobic, π–π electron-donor–acceptor, and charge–dipole interactions.[70,71] Other factors such as pore structure, functionality, nature of contaminants, and process conditions, such as temperature, pH, and competing ions can influence the mechanism and adsorption capacity of the adsorbents.[72] It is, therefore, paramount to choose an adsorbent that is highly selective to the target antibiotics.[73,74] A detailed scheme of the mechanism involved in the sorption of antibiotic molecules on a biochar material is simplified in the two pictorial illustrations in Fig. 3.

4.1 Removal of selected classes of antibiotics onto different biomass-based adsorbents

4.1.1 β-Lactam antibiotics. The efficacy of agricultural wastes that include eucalyptus leaves, wood ash, pine bark and needles, and crushed mussel shell has been scrutinized under optimum conditions for removing cefuroxime from wastewater.[75] A comparative study on the adsorptive removal of cefuroxime revealed that adsorbents such as wood ash and mussel shell that possessed pH values above 9 displayed the highest cefuroxime removal at the highest initial antibiotic concentration. This thereby indicated the simultaneous effect of pH on the chemical speciation of antibiotics and adsorbent surface that result in their electrostatic interactions.[75] Additionally, adsorption isotherm studies showed that cefuroxime removal best fitted both Freundlich and Langmuir models. On the other hand, the outcome of a desorption study revealed that eucalyptus leaves and pine bark displayed the highest desorption efficiencies of 28.6 and 26.6%, respectively. Another study by Naghipour *et al.* investigated the adsorption of cefixime from aqueous solutions by a biosorbent made from pine cones.[76] This study removed cefixime (CFX) from aqueous solutions using biochar made from pinecones. pH (2–12), contact length (0–120 min), initial CFX concentration (10, 50, and 100 mg L^{-1}), adsorbent dosage (0.1–2.5 g L^{-1}), and temperature (10 °C to 50 °C) were all investigated. The dry raw material was placed in a stainless steel reactor for carbonization and heated at 20 °C per minute in an electrical furnace for 2 hours at 460 °C. The samples were carbonized, then rinsed with distilled water and dried at 105 °C for 12 hours before being employed as an adsorbent. The biosorbent had a specific surface area of 789 m^2 g^{-1}, a total pore volume of 0.373 cm^3 g^{-1}, and a mean pore diameter of 1.89 nm. The removal efficiency was 92% when the circumstances were perfect (pH = 6.3, initial CFX concentration = 50 mg L^{-1}, contact period = 90 minutes, and adsorbent dosage = 2 g L^{-1}). This research showed that a biosorbent made from pinecones could be utilized to remove CFX from aqueous solutions and hospital wastewater cost-effectively and efficiently.

Table 3 Adsorptive removal performance of agricultural biomass-based adsorbents[a]

Material	Antibiotics	Pyrolysis condition/ activating agents	Experimental conditions	Adsorption capacity/removal efficiency	Kinetics	Isotherm	Mechanisms	Ref.
Red pine	Sulfamethoxazole SPY	400 °C	t = 72 h, pH = 6, T = 25 °C, dose = 10–15 mg	2.0	—	F	π–π electron-donor–acceptor (EDA) interaction	116
		500 °C		1.5				
Alfalfa *Medicago sativa* L.	Tetracycline	500 °C	pH = 5, t = 5 d, dose = 0.1 g L^{-1} conc. = 10–100 mg L^{-1}, T = 25 °C	372.31	PSOM	F	Surface complexation, hydrogen bonding and electrostatic interactions	68
Sugar cane bagasse	Chlortetracycline	500 °C	T = 25 °C, t = 24 h, pH = 5, conc. = 200 mg L^{-1}, dose = 10 g L^{-1}	16.96	PSOM	F	—	117
Wood	Tetracycline	800 °C	T = 298 K, t = 48 h, pH = 3.5–10.0, dose = 10 mg, conc. = 6.0–48 mg L^{-1}	163, 261	—	L	—	118
Rise husk	Tetracycline	H_2SO_4, KOH, 500–550 °C	T = 30 °C, dose = 5 g L^{-1}, conc. = 0.5–1 g L^{-1}	23.26, 58.82	PSOM	L	π–π interactions and hydrogen bonding	119
Treatment plant sludge	Tetracycline	NaOH, 700 °C	T = 25 °C, t = 8 d	124.8	—	L	—	120
Pinus taeda	Tetracycline	NaOH, 800 °C	T = 20 °C, t = 5 d, dose = 0.1g L^{-1}, conc. = 10–100 mg L^{-1}	434.36	Elovich	F	Hydrogen bonding and π–π interaction	73
Graphene-oxide bamboo sawdust composite	SMT	Graphene oxide, 600 °C	t = 24 h, pH = 3–9, conc. = 10 g L^{-1}, T = 25 °C	6.5	PSOM	F	p–p electron–donor–acceptor interaction	121
Cornhusk	Tetracycline, levofloxacin	$FeCl_3 \cdot H_2O$, 300 °C	t = 24 h, T = 30 °C, dose = 0.8 g L^{-1}, C = 266 mg L^{-1} (TC) 200 mg L^{-1} (LEV)	102	—	—	Hydrogen bonding and electrostatic attraction	122
Municipal solid waste sludge	Ciprofloxacin	Bentonite clay support, 450 °C	pH = 3–9, dose = 1.0 g L^{-1}, t = 12 h, conc. = 25 mg L^{-1}	286.6	PSOM, Elovich	Hill	Electrostatic interactions	91
Vinasse	Pefloxacin, ciprofloxacin	Manganese ferrite, 800 °C	pH = 3–10, T = 298 K, conc. = 1000 mg L^{-1}, dose = 0.1–2 g L^{-1}	256, 357	PSOM, Bangham fitting	L	Pore filling effect, π–π stacking interaction, π–π EDA, hydrogen bonding and hydrophobicity	123
Pomelo peel	Tetracycline, oxytetracycline, chlortetracycline	KOH, 400, 600 °C	Dose = 10 mg, conc. = 5–50 mg L^{-1}, t = 75 h, pH = 7, T = 294.15 K	476.19, 407.5, 555.56	PSOM	L	Pore filling, electrostatic interaction and π–π interactions	124
Fe/Zn-sawdust	Tetracycline	$FeCl_3 \cdot 6H_2O$, $ZnCl_2$, 600 °C	pH = 2–9, conc. = 40, 100, 150 mg L^{-1}	—	PSOM, Elovich	L	π–π EDA, hydrogen bonding	63

Table 3 (*Contd.*)

Material	Antibiotics	Pyrolysis condition/ activating agents	Experimental conditions	Adsorption capacity/removal efficiency	Kinetics	Isotherm	Mechanisms	Ref.
Chinese herb residue	Tetracycline, chlortetracycline, oxytetracycline	$ZnCl_2$, 500 °C	T = 303 K, dose = 0.02 g, conc. = 30–110 mg L^{-1}, pH = 3–10	188.7, 200.0, 129.9	PSOM	L	Hydrogen bonding and electrostatic interaction	72
Self-functionalized corncob biochar	Amoxicillin	Ultrasonic, 700 °C	t = 60 min, dose = 0.2 g	121.53	Elovich	F	π–π attractions	71
	Tetracycline			161.58				
	Levofloxacin			164.42				
Pomegranate wood			IC: 500 mg L^{-1}, dose: 0.04 g, pH: 6, T: 35 °C					79
(i) Activated carbon	Amoxicillin			234.6 mg g^{-1}	PSOM		Electrostatic attraction	
(ii) Activated carbon NH_4Cl-induced activated carbon	Amoxicillin			437 mg g^{-1}	PSOM	L	Electrostatic attraction	
Hazelnut-shell-derived activated carbon	Tetracycline		IC: 100 mg L^{-1}, dose: 0.1 g, pH: 5, T: 293 K	312.59 mg g^{-1}	PSOM	L	Hydrogen bonding and π–π interaction	94
	Oxytetracycline			322.60 mg g^{-1}	PSOM	L		
	Chlortetracycline			333.30 mg g^{-1}	PSOM	L		
Cow manure-based activated carbon	Sulfamethazine		Dose: 04 mg, pH: 3, T: 25 °C	3.62 mg g^{-1}	PSOM	F	—	125
Pine tree AC	Sulfamethoxazole		IC: 1.0 mg L^{-1}, dose: 0.003 g, pH: 3, T: 25 °C	131 mg g^{-1}	PSOM	L	—	88
KOH-modified pomegranate peel wastes	Ciprofloxacin		IC: 50–300 mg L^{-1}, dose: 0.025–0.2 g, pH: 2–12, t: 15–150 min, T: 25 °C	2.353 mg g^{-1}	—	F	Hydrogen bonding and π–π interaction	86
Activated carbon from	Ciprofloxacin		IC: 20 mg L^{-1}, dose: 0.05 g, pH: 8, time: 30 min		—	—	π–π interactions, hydrogen bonding and electron–donor–acceptor interaction	85
(i) Banana peel				31.67%				
(ii) Straw				93.34%				
(iii) Avocado peel				39.49%				
(iv) *Limonia acidissima* shell				23.43%				
(v) Tea waste				31.67%				
Pumpkin-seed-derived activated carbon derived	Ciprofloxacin		IC: 500 mg L^{-1}, dose: 0.04 g, pH: 6, T: 35 °C	234.6 mg g^{-1}	PSOM	L	Electrostatic attraction	79
				437 mg g^{-1}	PSOM	L	Electrostatic attraction	
Pomegranate wood			IC: 100 mg L^{-1}, dose: 0.1 g, pH: 5, T: 293 K				Hydrogen bonding and π–π interaction	94

Table 3 (*Contd.*)

Material	Antibiotics	Pyrolysis condition/ activating agents	Experimental conditions	Adsorption capacity/removal efficiency	Kinetics	Isotherm	Mechanisms	Ref.
(i) Activated carbon	Amoxicillin			312.59 mg g^{-1}	PSOM	L		
(ii) Activated carbon NH_4Cl-induced activated carbon	Amoxicillin			322.60 mg g^{-1} 333.30 mg g^{-1}	PSOM PSOM	L L		
(i) Eucalyptus leaves	Cefuroxime		IC: 2.5–50 μmol L^{-1}, dose: 0.5 g, *T*: 48 h	862.05 μmol kg^{-1}	NA	L–F	—	75
(ii) Wood ash				817.67				
(iii) Pine bark				700.09				
(iv) Pine needles				1223.47				
Lemna minor biomass	Ciprofloxacin		IC: 10 to 5 0 mg L^{-1}, time: 90 min, dose: 0.04 g, pH: 6, *T*: 273 to 323 K	19.62 mg g^{-1}	PSOM	NA	Physical adsorption	81
Sawdust	Ciprofloxacin hydrochloride		IC: 5–25 mg L^{-1}, dose: 1.0–5.0 g L^{-1}, pH: 3–12, *T*: 30 °C, *t*: 15–120 min	11.18 mg g^{-1}	PSOM	NA	Intra-particle diffusion	82
Modified sawdust Fe-coated sawdust	Tetracycline		IC: 10–20 mg L^{-1}, dose: 50 mg, pH: 2–10, *T*: 30 °C, *t*: 0–60 min	5.14 mg g^{-1}	PSOM	F	Electrostatic interaction hydrogen bonding	95
ZnO-modified pistachio shells	Amoxicillin		IC: 30–70 mg L^{-1}, dose: 0.1 g per 100 mL, pH: 3–9, *T*: 25–35 °C, *t*: 0–120 min	132.240 mg g^{-1}	PSOM	L	Chemisorption	114
	Ciprofloxacin			92.450 mg g^{-1}	PSOM	F	Intra-particle diffusion	
	Tetracycline			98.717 mg g^{-1}	PSOM	F		
Palm bark biomass	Amoxicillin		IC: 10–100 mg L^{-1}, dose: 0.5–5 g L^{-1}, pH: 6.5, *T*: 298 K, *t*: 10–180 min	35.92 mg g^{-1}	—	L	—	77
Magnetic chitosan graphene oxide composite	Ciprofloxacin		IC: 2–100 mg L^{-1}, dose: 10 mg, pH: 4–9, *t*: 0.08–8 h	282.9 mg g^{-1}	PSOM	L–F	Electrostatic attractions, π–π electron interaction	83
Modified indian almond biomass	Dicloxacillin		IC: 20–500 mg L^{-1}, dose: 0.025–3.0 g L^{-1}, pH: 2–8, *t*: 24 h, *T*: 273.15–323.15 K	71.94 mg g^{-1}	PSOM	L	Hydrogen bonding, van der Waals forces	80
Moringa oleifera	Oxytetracycline		IC: 0.2–1.0 mg L^{-1}, dose: 1–2 g L^{-1}, *t*: 5–120 min, *T*: 20–40 °C	50.3%	PSOM	F	Electrostatic attractions intra-particle diffusion	92
Spent mushroom substrates	(i) Sulfamethyldiazine		IC: 0.5–10 mg L^{-1}, dose: 1–2 g L^{-1}, pH: 1–11	2.1072 mg g^{-1}	PSOM	L	—	87
	(ii) Sulfamethazine			1.8103 mg g^{-1}				
	(iii) Sulfathiazole			2.2991 mg g^{-1}				

Table 3 (*Contd.*)

Material	Antibiotics	Pyrolysis condition/ activating agents	Experimental conditions	Adsorption capacity/removal efficiency	Kinetics	Isotherm	Mechanisms	Ref.
	(iv) Sulfamethoxazole			2.2133				
Magnetic functionalization of sugar cane bagasse	Tetracycline		IC: 0–200 mg L^{-1}, dose: 0.05 g, *t*: 0–25 h, *T*: 30 °C, pH: 6.8	48.35 mg g^{-1}	PSOM	F	Hydrogen bonding and π–π interaction	126
Grape slurry (activated carbon from grape slurry)	Chloramphenicol	650 °C	23 ± 2 °C, 150 rpm, dose = 0.10 g		PSOM	L and F		104
Corn stalk biomass fiber & Fe_3O_4 embedded chitosan	Chloramphenicol		35 °C, reaction time = 3 h, dose = 30 mg	58.75 mg g^{-1}	PSOM	L		102
Porous carbon from waste lignin	Chloramphenicol	800 °C	Dose = 120 mg L^{-1}	534.0 mg g^{-1} at 303 K	PSOM	L		103
Biochar from peanut shell	Chloramphenicol (CHLR)	105 °C for 12 h	Natural pH, 25 °C, 180 rpm, conc. = 100, 300, 600 mg L^{-1}, dose = 1.0 g L^{-1}	423.7 mg g^{-1} and 90%	PSOM	L	Hydrogen bonding interaction π–π interaction	105
Date palm fiber	Tyrosine		IC: 10 to 5 0 mg L^{-1}, time: 90 min, dose: 0.04 g, pH: 6, *T*: 273 to 323 K	147	PSOM	L	Electrostatic, H-bonding, π–π EDA interaction	97
Corchorus capsularis	Tyrosine		IC: 10 to 5 0 mg L^{-1}, time: 90 min, dose: 0.04 g, pH: 4–7, *T*: 273 to 323 K	25	PSOM	L	Hydrophobic, electrostatic, H-bonding, π–π EDA interaction	97
Banana peel graphene	Erythromycin			286	PSOM	L	N/A	97
Cotton gin waste and guayule bagasse biochar	Erythromycin			17.12	PSOM	L	Hydrophobic partitioning, H-bonding and π–π interactions	97
Cuttlefish bone powder	Clarithromycin			34.5	PSOM	F	Electrostatic interaction	
Rice husk	Azithromycin		IC: 100 mg L^{-1}, time: 0–250 min, dose: 0–20 g, pH: 4–7, *T*: 300 K	612.22	PFOM	L	N/A	99
	Erythromycin			599.72		L	N/A	
Corn cobs	Tyrosine		IC: 20–100 mg L^{-1}, time: 5–540 min, dose: 0–20 g, pH: 6, *T*: 298, 308, 318 K	14.0	PSOM	L	N/A	100

Table 3 (*Contd.*)

Material	Antibiotics	Pyrolysis condition/ activating agents	Experimental conditions	Adsorption capacity/removal efficiency	Kinetics	Isotherm	Mechanisms	Ref.
Azolla filiculoides – based activated porous carbon	Azithromycin		IC: 25–200 mg L^{-1}, time: 0–180 min, dose: 0.1–1.5 g, *T*: 273–325 K	374	PSOM	L	Physical adsorption	101
Feather-derived charcoal	TMC	600 °C	pH: 2–12, *T*: 293, 303 and 313 K, *t*: 0–60 h, dose: 0.2 g, IC: 1000 mL	164 mg g^{-1}	Intraparticle diffusion, PS1 and PS2	L, F and DR	Exothermic and electrostatic interaction	112
Modified peanut husk with betaine (MPN-Bet)	TMC	Co-precipitation, 60 °C	pH: 2–11, dose: 0.005 to 0.05 g, *t*: 0–350 min, *T*: 293, 303 and 313 K, IC: 0–0.1 mol L^{-1}	31.2 ± 3.2 mg g^{-1}	Intraparticle diffusion, PS1 and PS2	L, F and T	Chemisorption	111
Waste citrus peel	TMC	NA	IC: 50–150 mg L^{-1}, pH: 4–10, *T*: 293–323, dose: 0.05–0.15 g	144.9 mg g^{-1}	PS1 and PS2	L and F	Chemisorption	113
Red pine	SMX	400 °C	$t = 72$ h, pH = 6, $T =$ 25 °C, dose = 10–15 mg	2.0	—	F		116
	SPY	500 °C		1.5				
Alfalfa *Medicago sativa* L.	TC	500 °C	pH = 5, $t = 5$ d, dose = 0.1 g L^{-1}, conc. = 10–100 mg L^{-1}, $T =$ 25 °C	372.31	PSOM	F		68
Waste rice straw	TCS	300 °C	$t = 30$ min, dose = 50 mg L^{-1}, conc. = 10–50 mg L^{-1}, $T =$ 25 °C	714	PSOM	L		106
Kenaf biochar	TCS	750 °C	pH = 5, $t = 24$ h, dose = 0.03 g L^{-1}, conc. = 30 mg L^{-1}, T = 25 °C	77.4 mg g^{-1}	PSOM	L		107
Magnetic carbon composites	TCS	27 °C	$t = 10$ min, dose = 50 mg L^{-1}, conc. = 10–50 mg L^{-1}, $T =$ 30 °C	892.9 mg g^{-1}	PSOM	L		127
Microwave-activated biochar	Lincomycin	105 °C	pH = 3 to 10, conc. = 50 mg L^{-1}, dose = 1 g L^{-1}, temp = 25 °C	190 mg g^{-1}	Pseudo-second-order	Redlich–Peterson	Electrostatic interaction	109

[a] F = Freundlich, L = Langmuir, T = Temkin, IC = initial concentration, *t* = time, *T* = temperature, PSOM = pseudo-second-order model, PFOM = pseudo-first-order model.

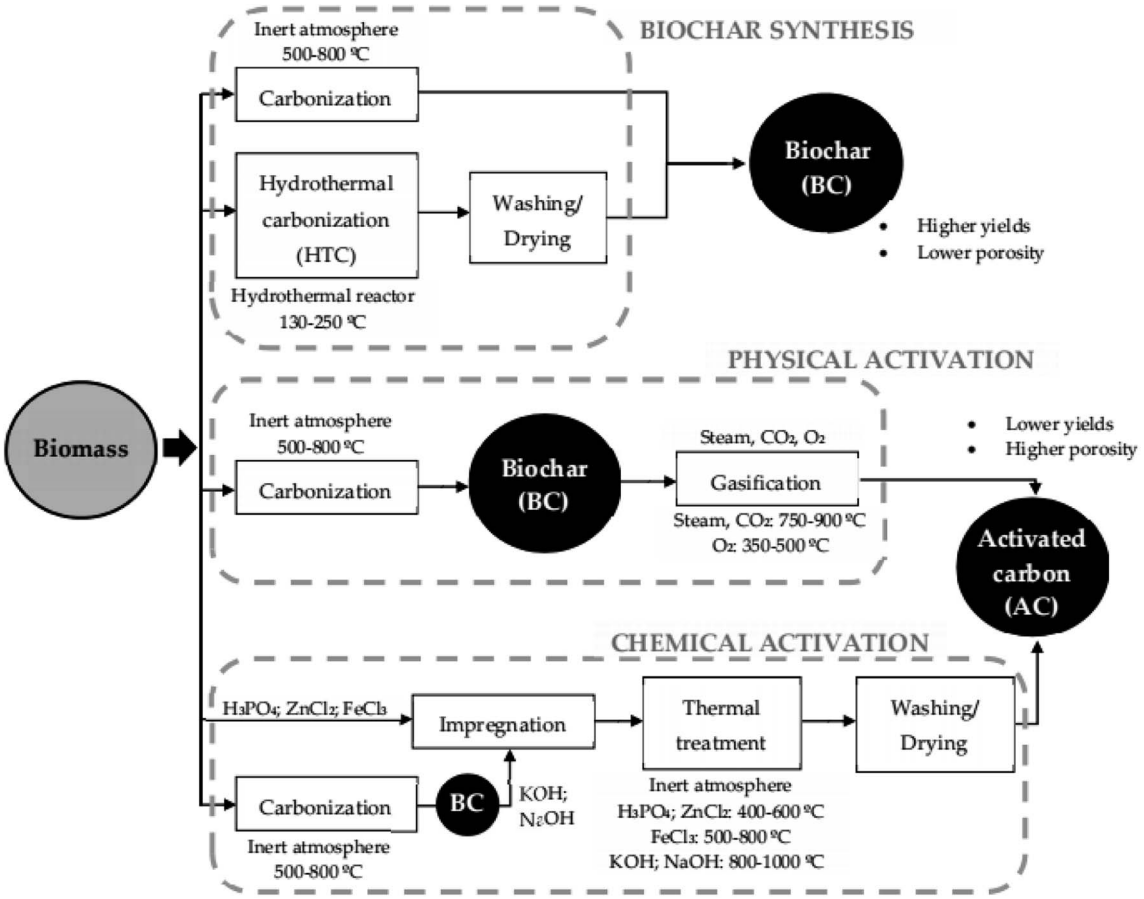

Fig. 2 Synthetic route for preparing biochar and activated carbon from biomass.[66]

Another biomass, palm bark, was utilized under adsorption conditions of 0.5 to 5 g L^{-1} (adsorbent dosage), 10 to 100 mg L^{-1} (initial concentration), and 10 to 180 min (contact time) for amoxicillin removal.[77] Furthermore, the palm bark biomass was shown to yield 98.1% removal of amoxicillin at 90 min contact time, 3 g L^{-1} adsorbent dose and 10 mg L^{-1} of amoxicillin at a solution temperature of 25 °C. Additionally, the adsorption isotherm for palm bark biomass in removing amoxicillin from an aqueous solution was inferred to be best interpreted using the Langmuir model, compared to the Freundlich and Temkin isotherm models.[77] Moreover, it was suggested from the experimental findings that there was an increase in the percentage removal of amoxicillin when the adsorbent dose was increased from 0.5 to 3.0 g because of the availability of binding sites positioned on the adsorbent surface. In contrast, there was no significant upsurge in the percentage removal of amoxicillin when there was a further increase in the adsorbent dosage as a result of the diminution of the amoxicillin concentration. In addition, there was a rapid removal of amoxicillin at the initial phase of contact period, but it subsequently became slower when approaching equilibrium.[77] The rate of amoxicillin adsorption between the initial phase of contact time and equilibrium time was reported to be virtually constant as a result of the large number of binding sites located on the adsorbent surface, compared to the reduced number of binding sites after a lapse of time. The decrease in the number of binding sites obtained on the adsorbent surface resulted in repulsive forces between the amoxicillin ions and a resultant decline in the percentage removal of amoxicillin using palm bark biomass. Similarly, an increase in the initial amoxicillin concentration was inferred to result in a decrease in the percentage removal of amoxicillin, consequent to the saturation of the binding sites of the palm bark biomass at a fixed dose.[77]

Activated carbons derived from lignocellulosic precursors obtained from olive stones have been crucially utilized in removing amoxicillin from wastewater.[78] The speedy adsorption kinetics were supposedly controlled by a pseudo-second-order model and were ascribed to the presence of an immense network of mesopores on the activated carbons. The rapid adsorption kinetics is an indication that there is no constraint on the accessibility of pores on the activated carbon surface. This outcome agreed closely with the molecular dimension of amoxicillin (ca. 1.24 × 0.56 × 0.46 nm), as computed from 3D optimization for the lowest energy configuration using Chem Sketch software.[78] Similarly, investigation of the employment of activated carbon derived from NH_4Cl-modified pomegranate wood in removing amoxicillin has been reported.[79] The adsorptive capacities of unmodified and NH_4Cl-modified activated carbons were suggested to be 262 and 437 mg g^{-1}, and the effective adsorption process was attributed to the high surface

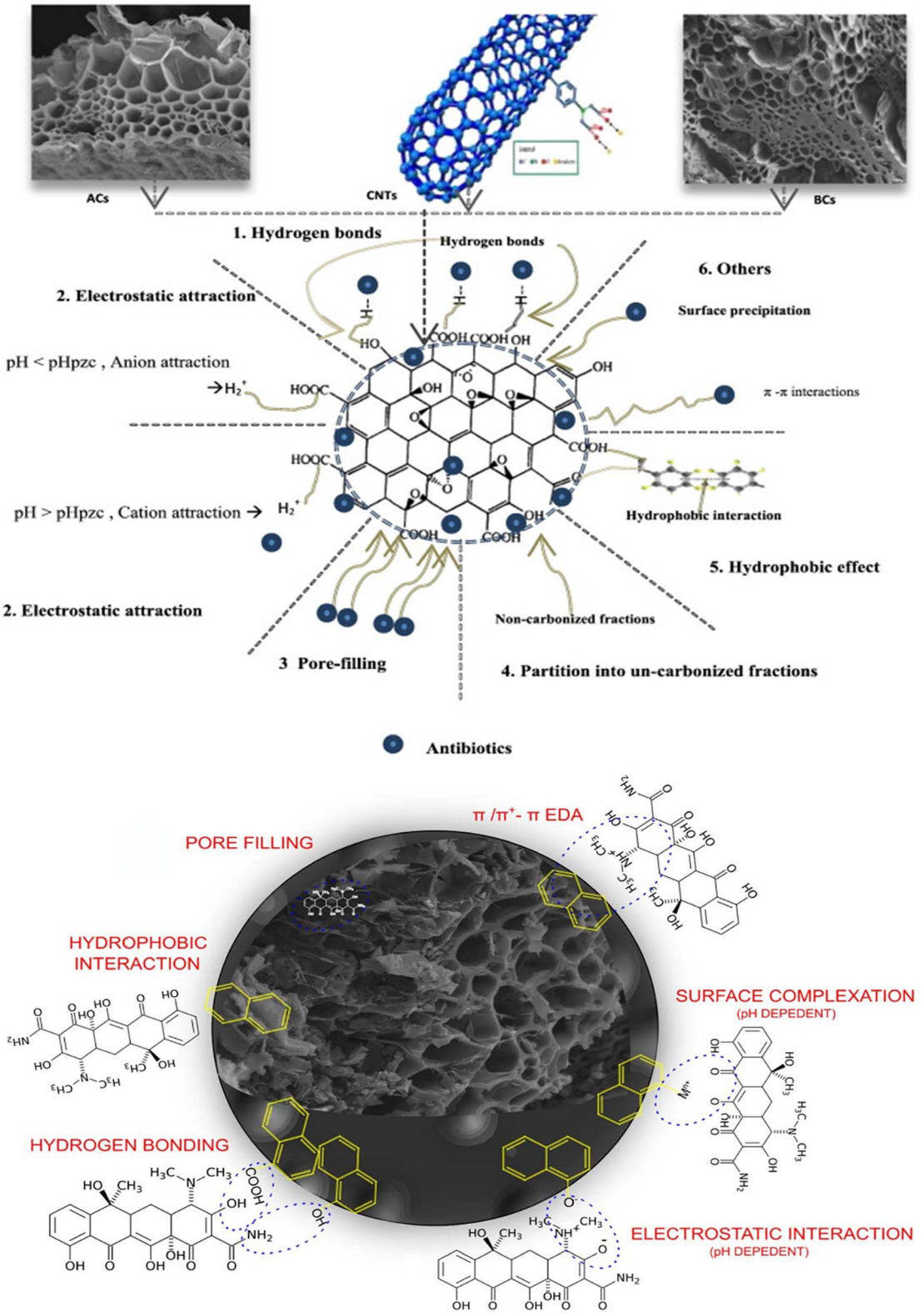

Fig. 3 A detailed scheme of the mechanism involved in the sorption of antibiotic molecules on a biomass-based material.[25,33]

area, functional groups, and interaction between the modified adsorbent and amoxicillin, which was pH-dependent.[79] Moreover, the experimental findings established the existence of electrostatic interaction between the positively charged functional groups on the cationic surfactant of the adsorbent and carboxyl anions in the structure of amoxicillin antibiotic

molecules as the governing mechanism of the adsorption process. Comparatively, the unmodified and NH_4Cl-modified activated carbon respectively displayed 55 and 99% amoxicillin removal at optimum adsorption conditions with Langmuir and pseudo-second-order giving the best interpretation for the adsorption isotherm and kinetics, respectively.[79]

In another study, the modification of indian almond biomass with the use of concentrated acid and sodium bicarbonate solution has been investigated in preparing tannin to act as a suitable adsorbent for removing dicloxacillin from water.[80] The impact of pH on utilizing tannin for removing dicloxacillin was studied as the percentage removal of dicloxacillin increases with an increase in pH from 2 to 6. This outcome was linked to the increase in the degree of ionization of phenolic hydroxyl ions of tannin that increases with pH, thereby resulting in higher removal of dicloxacillin.[80] Contrariwise, there was a decrease in the percentage removal of dicloxacillin at pH values that exceeded 6. Furthermore, it was reported that there was a quick adsorption removal of dicloxacillin on tannin during the initial phase of contact time, but equilibrium was attained at 24 h of contact time.

4.1.2 Fluoroquinolone antibiotics. Ciprofloxacin removal from an aqueous medium by utilizing *Lemna minor* biomass has been suggested to display adsorption kinetics best defined with the pseudo-second-order model demonstrating adsorption capacities ranging from 4.31 to 19.62 mg g^{-1} for an initial ciprofloxacin concentration range of 10 to 5 0 mg L^{-1}.[81] Furthermore, thermodynamic studies revealed that the percentage removal of ciprofloxacin consistently increased from 72.41 to 91.6% with increasing solution temperature from 273 to 323 K, thereby yielding an endothermic and spontaneous chemical reaction. In addition, a kinetics study deduced that equilibrium with the optimum adsorption of ciprofloxacin was attained in 90 min of contact time. This rapid adsorption removal of ciprofloxacin was ascribed to the large number of available active sites situated on the adsorbent surface. However, a slower adsorptive removal of ciprofloxacin was recorded at a higher contact time, resulting from the lower numbers of active sites positioned on the adsorbent surface after 90 min of contact time.[81] In another study, the employment of unmodified sawdust has been reported for removing ciprofloxacin from wastewater. Experimental findings revealed that the contact time required to attain equilibrium removal of ciprofloxacin was dependent on the initial concentration of ciprofloxacin.[82]

Rapid removal of ciprofloxacin of about 80% was noted within the first 5 min of the adsorption process. Conversely, beyond 5 min, the removal of ciprofloxacin was noted to be slow and, lastly, equilibrium was reached within 40 to 60 min of contact time. The result from pH studies signified that the removal of ciprofloxacin increased with an increase in pH until an equilibrium capacity of 11.6 mg g^{-1} was attained at pH 5.8.[82] Beyond this, there was a steady decrease in the removal of ciprofloxacin with a respective increase in the solution pH of the adsorption process. Furthermore, the effect of the sawdust/ciprofloxacin ratio was reported to impact the percentage removal of ciprofloxacin. An increase in percentage ciprofloxacin removal was suggested to occur with a corresponding increase in the sawdust/ciprofloxacin ratio until equilibrium was reached at a ratio of 2.0, beyond which there was no further increase in the removal of ciprofloxacin.[82] This finding was ascribed to occupation by ciprofloxacin on the active sites of the sawdust adsorbents, thereby preventing further removal of ciprofloxacin from the solution. Additionally, the kinetics and the mechanism for ciprofloxacin removal using sawdust were supposedly controlled by a pseudo-second-order model and intra-particle diffusion process, respectively. At the same time, regeneration studies revealed 85% efficiency compared to the initial adsorption capacity in removing ciprofloxacin.[82]

Chitosan is a linear cationic amino-polysaccharide composed of α-D-glucosamine, which can be obtained from chitin naturally occurring in relative abundance. Reports on the modification of chitosan have been conveyed as obtaining a magnetic chitosan graphene oxide composite as a viable adsorbent for removing ciprofloxacin from wastewater.[83] By reason of the magnitude of solution pH on the surface charge of adsorbents as well as speciation of adsorbate ions in circulation, the effect of pH on ciprofloxacin elimination has been reportedly regulated by electrostatic and π–π attraction. It was reported that the removal of ciprofloxacin decreases with pH values above 5, which was reported as the optimum pH for removing ciprofloxacin with modified chitosan.[83] Similarly, a decrease in ciprofloxacin removal was reported when the solution pH decreased from 5 to 4. This observation can best be explained based on the existence of ciprofloxacin in the mostly cationic form at pH <6.1 and the anionic form of ciprofloxacin existing at pH >8.7, while in the pH range of 6.1 to 8.7, ciprofloxacin exists as zwitterions. The adsorptive removal of ciprofloxacin on modified chitosan was reported to be swayed by the existence of metal ions following the 40.9 and 37.5% declines in ciprofloxacin removal under the influence of calcium as well as sodium ions,[83] consequently confirming the influence of electrostatic attraction on the adsorption removal of ciprofloxacin. In addition, the utilization of modified chitosan on removing ciprofloxacin was best interpreted with the Langmuir isotherm model with a maximum adsorption capacity of 282.9 mg g^{-1}, but kinetically controlled by the pseudo-second-order model. Lastly, 72% of the preliminary adsorption capacity in removing ciprofloxacin was reported after four cycles of reuse from regeneration studies.[83]

Correspondingly, activated carbon derived from pumpkin seed has been employed in removing ciprofloxacin antibiotics from wastewater.[84] The experimental outcome shows that pumpkin-seed-based activated carbon displayed 99% removal of ciprofloxacin antibiotics under optimum experimental conditions. The adsorption isotherm was best interpreted using the Langmuir model with a physical adsorption path, while the findings from thermodynamics confirmed an endothermic and spontaneous adsorption process.[84] Similarly, the utilization of KOH has been explored as an activating agent for preparing activated carbons derived from agricultural wastes that include banana peel, straw, avocado peel, *Limonia acidissima* shell, and tea waste to remove ciprofloxacin.[85] The experimental results

revealed that the straw-based-activated carbon presented the highest adsorption removal of ciprofloxacin at 93.34%, whereas the *Limonia acidiss*ima shell-based activated carbon displayed the least adsorption removal of ciprofloxacin at 23.43%.[85] Further insight into the adsorption process disclosed that the presence of hydroxyl, carboxyl, and carbonyl ester groups on the activated carbons plays a dynamic part in the binding of activated carbon to the ciprofloxacin molecules. This promotes the adsorption of ciprofloxacin on the activated carbon *via* π–π interactions and hydrogen bonding as well as an electron-donor–acceptor mechanism.[85]

Another activated carbon derived from KOH-modified pomegranate peel wastes for ciprofloxacin removal from aqueous system has been reported.[86] The experimental findings revealed an optimum pH of 8, and recounted a high level of protonation on the adsorbent surface at lower pH that expedited electrostatic attraction between ciprofloxacin and the prepared activated carbon. Similarly, an optimum dose of 0.05 g was suggested from the experimental findings to yield the highest adsorption capacity, whereas there was a major decline in adsorption removal of ciprofloxacin at a higher adsorbent dose.[86] Moreover, rapid adsorption removal of ciprofloxacin was attained within a contact period of 30 min, after which there was no significant increase in the adsorption removal of ciprofloxacin at a higher contact time. This outcome is consequent on the high initial concentration gradient occurring between the adsorbates and the number of unoccupied active sites on the adsorbents. In addition, the adsorption isotherm for removing ciprofloxacin was best interpreted with the Freundlich model, compared to the Langmuir model which produced a maximum adsorption capacity of 2.353 mg g^{-1}.[86]

Investigation on the adsorption of ciprofloxacin (CIP) onto composite derived from solid waste supported on bentonite clay was carried out by Ashiq *et al.*[91] A 40% increase in removal efficiency of CIP was reported compared with bare BC, which was attributed to the intercalation of CIP in the clay–BC layer. In addition, the improved active pores and existence of electrostatic attraction between the functional groups of CIP molecules and the BC composites favored increased removal efficiency. Experimental data best fitted the Hill isotherm alongside pseudo-second-order and Elovich kinetic models. The optimum adsorption capacity of 190 mg g^{-1} was attained at pH 6.

4.1.3 Sulfonamide antibiotics. Investigative studies on the removal of sulfamethoxazole and other sulfa antibiotics by means of unmodified spent mushroom substrate have been reported to yield insignificant adsorption capacity.[87] Nevertheless, hydrogen bonding occurring between the N-hetero-aromatic ring of sulfamethoxazole as well as the surface of the unmodified spent mushroom substrate was posited to be the mechanism governing the adsorption process.[87] Tonucci *et al.* (2015) recounted the removal of sulfamethoxazole using an adsorbent obtained from the modification of coconut shell and *Pinus* tree.[88] The experimental findings documented the existence of electrostatic attraction as the dominant force governing the adsorption process, whereas the Langmuir model gave the best fit for the adsorption isotherm. This indicated a monolayer formation of sulfamethoxazole on the surface of the modified adsorbents.[88]

Sulfamethoxazole (SMZ) sorption from an aqueous solution was achieved using *Azolla filiculoides* (AF) as an adsorbent.[89] Adsorption came into play as well. Thermodynamics, isotherms, and kinetics were investigated. During the experiments, the contact time, agitation speed, initial SMZ concentration, and temperature were varied. The Langmuir, Freundlich, and Temkin adsorption isotherms were all investigated. The Langmuir models were the best fit for describing SMZ sorption in aqueous solutions (because of their high R^2 values). Pseudo-first-order, pseudo-second-order, and intra-particle diffusion models were all used to fit the experimental data. The pseudo-second-order kinetic model was more accurate than other kinetic models in describing the adsorption process. Standard free energy changes (G), standard enthalpy change (H), and standard entropy change (S) were all determined as thermodynamic parameters. The adsorption of SMZ on AF biomass was found to be practicable, spontaneous, and endothermic based on these criteria. This research discovered that AF biomass is an effective adsorbent for removing sulfamethoxazole antibiotics from an aqueous solution.

Kurup in 2012 (ref. 90) reported the adsorption removal of sulfamethoxazole using an alkali (NaOH)-treated agricultural-waste-based adsorbent obtained from deoiled soya. Compared to unmodified deoiled soya, the display of the hydroxyl group and the accessibility to a higher surface area were demonstrated by the alkali-modified deoiled soya. Besides, the detected decline in the porosity of the alkali-modified deoiled soya was ascribed to the occurrence of sodium ions. Nonetheless, the alkaline modification ensued in an increase from 10 to 20% of sulfamethoxazole exclusion and the adsorption mechanism was well defined by dint of electrostatic force and ion exchange.[90]

Similarly, Huang *et al.*[121] investigated a GO-modified bamboo sawdust biochar composite for sulfamethazine (SMT) adsorption. The FTIR spectra showed more oxygen functional groups on the composite surface, which was also reflected in the SBET due to GO addition. The sorption of SMT onto GO–BC was best described by the Freundlich isotherm with $R^2 = 0.969$, indicating the existence of electrostatic interactions in the core of the heterogenous active sites in the composite. Other mechanisms such as hydrogen bonding and cation exchange were suggested to support the adsorption. This established the potential of GO–BC nano-composites for antibiotic removal.[121]

4.1.4 Tetracycline antibiotics. The efficiency of *Moringa oleifera* shells for removing oxytetracycline antibiotics from wastewater at an optimum adsorption process has reportedly been studied. The outcome of the pH findings on removing oxytetracycline indicated a pH-dependent adsorption process, which reflected a corresponding increase in adsorbed oxytetracycline with an increase in solution pH from 3 to 10.[92] The low adsorption removal of oxytetracycline at pH 3 was attributed to electrostatic repulsion, while the increase in oxytetracycline removal at alkaline pH was attributed to electrostatic attraction. This proposition was centered on the occurrence of oxytetracycline in its anionic and cationic forms at pH >7.32 and pH <3.27, respectively, while the zwitterion of oxytetracycline was found in

a pH range of 3.27–7.32, thereby confirming the insufficient affinity between *Moringa oleífera* shells and oxytetracycline.[92] Likewise, the adsorption removal of oxytetracycline reportedly increased with increasing initial concentration of oxytetracycline, thereby indicating that the effect of initial concentration is negligible on using *Moringa oleífera* shells for removing oxytetracycline. Correspondingly, an increase in solution temperature resulted in increasing oxytetracycline removal, with the maximum adsorption removal reported at 40 °C. However, there was a negligible difference between the adsorption capacities obtained at solution temperatures of 20 and 40 °C.[92] In addition, the Freundlich model gave the best description for the adsorption isotherm for utilizing *Moringa oleífera* shells to remove oxytetracycline. Moreover, the kinetics of removing oxytetracycline by using *Moringa oleífera* shells revealed that only 34% of the initial oxytetracycline concentration was removed after 2 h. This denotes that the adsorption process is pH-dependent and there is insufficient affinity between *Moringa oleífera* shells and oxytetracycline. Finally, the adsorption mechanism for oxytetracycline removal was stated to be pH-dependent and kinetically controlled by dint of the intra-particle diffusion model with a correlation coefficient of 0.9506.[92]

Activated carbon derived from hazelnut shell for the elimination of tetracycline, oxytetracycline and chlortetracycline yielded 312.59, 322.60 and 333.30 mg g^{-1} adsorption capacities controlled by hydrogen bonding as well as a π–π interaction adsorption mechanism with an endothermic adsorption process. Furthermore, the maximum adsorption capacities of hazelnut-shell-derived activated carbon was obtained under optimum conditions of 5 (pH), 293 K (temperature) and 0.1 g (adsorbent dose) with the adsorption isotherm and kinetics best described using Langmuir and pseudo-second-order models, respectively.[67,93,94] In 2020, Wang *et al.* synthesized a zinc–chloride–activated biochar derived from *Flueggea suffruticosa* to adsorb oxytetracycline (OTC), tetracycline (TC) and chlortetracycline (CTC) from aqueous solution. The surface area was found to be 2556 m^2 g^{-1}, and the isotherm data fitted well to the Langmuir model, which assumed monolayer adsorption occurred while kinetics were correlated best to pseudo-second-order. At 30 °C the maximum adsorption capacities of Zn–BC were 200, 188.7 and 129.9 mg g^{-1} for TC, CTC and OTC, respectively. From the thermodynamic studies, the entropy value was found to be positive while ΔG^0 was negative, which is an indication of spontaneity. In addition, it also revealed that the adsorption of TC and CTC was an endothermic process, whereas that of OTC was exothermic from the negative and positive ΔH^0 values obtained. In summary, at a wider pH and ionic strength range, Zn–BC had a larger adsorption capacity for TCs. Thus, Zn–BC is a prospective material for removing pollutants in an environmental manner.[72]

Alidadi[95] demonstrated an improvement in adsorption capacity for removing tetracycline by using modified sawdust in the sequence order of $FeCl_3$ > HCl > $CaCl_2$ > $NaHCO_3$ modifying agents. Furthermore, the utilization of $FeCl_3$ for modifying sawdust yielded accessible, functional groups that include carboxylic, ferric, carboxylate and hydroxyl by means of the existence of oxygen, carbon and iron atoms on the surface of the sawdust. The demonstration of a pH of 4.15 by the modified sawdust denotes a positively and negatively charged surface of modified sawdust at pH values below and above 4.15, respectively, and a modified sawdust surface with a neutral charge at pH 4.15.[95] A comparable trend in pH studies was reported when sulfonation-modified sawdust was experimented with in removing tetracycline with maximum adsorption capacity obtained at a neutral pH.[96] A sulfonation modifying agent has been noted to generate a sulfur deposit on the surface of sawdust. It yielded sulfonic acid groups (–SO_3H) that support the adsorption of tetracycline on sulfonation-modified sawdust *via* the mechanisms of electronic interaction, π–π interaction, and hydrogen bonding.[96]

4.1.5 Macrolide antibiotics. The use of biomass-based adsorbent for the removal of macrolide antibiotics (such as clarithromycin, erythromycin, azithromycin) has been reported to yield maximum adsorption capacities in the range of 7.56–340 mg g^{-1}. The employment of adsorbents derived from date palm fiber, *Corchorus capsularis*, banana peel graphene, cotton gin waste, guayule bagasse biochar and cuttlefish bone powder have been suggested to be effective for the removal of macrolide antibiotics from wastewater.[97] The adsorption process for removing tyrosine antibiotics using adsorbents derived from date palm fibre and *Corchorus capsularis* was suggested to proceed with pseudo-second-order adsorption kinetics and the adsorption isotherm was best described using the Langmuir isotherm model with maximum adsorption capacities of 147 and 25 mg g^{-1}, respectively.

Furthermore, the adsorbents derived from banana peel graphene, cotton gin waste and guayule bagasse biochar have been reported to be effective for the removal of 286 and 17.12 mg g^{-1} of erythromycin, respectively. In addition the adsorption kinetics and isotherm were best described using the pseudo-second-order and Langmuir models.[97,98] The adsorption removal of clarithromycin from pharmaceutical effluent by employing an adsorbent derived from cuttlefish bone powder has been posited to yield a maximum adsorption capacity of 34.5 mg g^{-1} with an electrostatic mechanism. However, the adsorption kinetics and isotherm were best interpreted using pseudo-second-order and the Freundlich model.[97]

The employment of a low-cost adsorbent obtained as a biochar derived from rice husk at a temperature range of 450–600 °C has been effective for removing more than 95% of azithromycin and erythromycin from pharmaceutical effluents.[99] Maximum adsorption capacities of 612.22 and 599.72 mg g^{-1} for the respective removal of azithromycin and erythromycin were reported using rice husk biochar derived at temperatures of 500 and 600 °C, respectively.[99] The use of adsorbent derived from agricultural waste corn cobs has been successfully reported to yield a low adsorption capacity of 14.4 mg g^{-1} for removing tyrosine antibiotics using the Langmuir model which best described the adsorption process. However, the adsorption kinetics for the removal of tyrosine was best described using a pseudo-second-order model.[100]

The utilization of *Azolla filiculoides*-based activated porous carbon has been recommended to be effective in removing 87

and 98% of azithromycin after respective adsorption contact times of 75 min, at 303 and 333 K.[101] Furthermore, the adsorption removal of azithromycin was endothermic and spontaneous with the adsorption isotherm best described using the Langmuir model with an adsorption capacity of 374 mg g^{-1}, while the adsorption kinetics was best described using the pseudo-second-order model.[101]

4.1.6 Chloramphenicol. In a recent study by Xing *et al.*,[102] a biomass-based adsorbent, based on corn stalk fiber and Fe_3O_4-embedded chitosan (CS), was used to remove chloramphenicol. The viability of adopting these adsorbents to extract chloramphenicol from aqueous solution was estimated. There is a chance that corn stalk fiber and Fe_3O_4-embedded chitosan will be viewed as an effective and cost-effective material for removing chloramphenicol from the aquatic environment. Compared to the Freundlich model, the Dubinin–Radushkevich model, and the Temkin model, the Langmuir model provided a superior fit for the adsorption isotherms derived from batch experiments while the adsorption kinetic data agreed well with the pseudo-second-order kinetic model. Adsorbent thermodynamic adsorption tests were also carried out at 298, 308, and 318 K. The study showed that there is a chance that corn stalk fiber and Fe_3O_4-embedded chitosan will be viewed as a very good and cost-effective material for removing chloramphenicol from the aquatic environment.[102]

Another study investigated the removal of chloramphenicol from water using porous carbon materials extracted from waste lignin.[103] The highest adsorption capacity of this adsorbent at a starting concentration of chloramphenicol of 120 mg L^{-1} was 534.0 mg g^{-1} at 303 K. The adsorption capacity did not change significantly under a pH of 4.86, so the initial pH was chosen as the ideal condition for the future tests. In this study, the adsorption process of chloramphenicol was endothermic and spontaneous, according to a thermodynamic analysis of the adsorption isotherm. The high adsorption capability of the synthetic adsorbents was maintained in a complex aquatic environment, which was remarkable. It was concluded from the study that the porous carbon as adsorbent was a cheap and productive biomass-based adsorbent with a wide range of potential applications and it is also easy to use.[103]

A study on the removal of chloramphenicol from contaminated water using adsorbents made from grape slurry waste has been reported.[104] A batch experiment was carried out using simulated antibiotic-contaminated water. According to the study, waste grape slurry could be a useful starting point for creating efficient adsorbents for treating wastewater polluted with antibiotics. Temperature variations appeared to have an impact on the affinity of antibiotics for the adsorbent surface which demonstrated that when the temperature of the solution increases, the adsorption capacity of the adsorbents increases. Thermodynamic analyses also revealed that the sorption of CHLR was an exothermic reaction that was conceivable but not spontaneous as the temperature rose.[104]

The adsorptive removal of antibiotic contaminants from wastewater using biochar from peanut shells was studied.[105] In this study, chloramphenicol served as the reference antibiotic. Waste biomass was pyrolyzed using small amounts of ammonium polyphosphate to create porous biochar that can bind with chloramphenicol. The nitrogen and phosphorus of ammonium polyphosphate additionally encouraged the chemical activity of biochar surface. The Langmuir model and the pseudo-second-order model of chloramphenicol adsorption were the best fits. The study presented alternative routes to biochar preparation and also additional applications of biochar in antibiotic removal.

4.1.7 Antiseptic additives. One biocide, triclosan (TCS), has the ability to both eradicate and stop the growth of microorganisms. It functions as an antibacterial, antifungal, and antimicrobial agent. As a result, it can be found in a variety of personal care and health goods, including deodorant, detergent, cosmetics, first aid, and shampoo. TCS, on the other hand, has the potential to harm human health and the environment through endocrine disruption, acute toxicity, and environmental pollution. It was found in numerous wastewater treatment facilities, soil, and rivers as a result of accelerated urbanization and population increase. The traditional method for removing TCS and other water contaminants required numerous chemicals, took a long time, and was ineffective at getting rid of all the pollutants.

Liu *et al.*[106] considered discarded rice straw which is hydrothermally liquefied (HTL) to create hydrochar. However, because of its small porosity and surface area, hydrochar material could not be used directly in the environmental field. The hydrochar produced from rice straw was therefore activated and magnetized to create magnetic activated carbon in order to increase the porosity and adsorption capability. The detrimental impact of the magnetic medium led researchers to first explore the activation requirement for hydrochar. The results showed that the magnetically activated carbon has a large surface area (about 674 m^2 g^{-1}), a high adsorption capacity, and a rapid adsorption rate for the removal of triclosan (TCS). An external magnetic field can also be used to recover magnetically activated carbon quickly from aqueous solutions. Overall, the hydrochar made from discarded rice straw may be converted into a very effective magnetic adsorbent for TCS elimination.

Recently, Cho *et al.*[107] examined how triclosan can be removed from an aqueous solution using biochar made from kenaf. Physical and chemical analyses were used to investigate the triclosan adsorption process of biochars that were pyrolyzed at different temperatures (300, 400, 600, and 750 °C) (FE-SEM, EDS, EA, XRF, pHpzc, N_2 adsorption–desorption, SAXS, ATRF-TIR, and XPS). As the pyrolysis temperature climbed, triclosan adsorption by the kenaf biochar improved, with the exception of 450 °C, which showed the least sorption capacity. The maximum sorption capability was demonstrated by kenaf biochar produced at 750 °C (KNF-750), which had a high aromatic moiety and a sizable specific surface area. The pseudo-second-order model accurately described the kinetic adsorption of KNF-750, with equilibrium being reached in 3 hours. The maximum triclosan adsorption capacity for KNF-750 of the Langmuir model, which had a strong correlation coefficient, was 77.4 mg g^{-1}. Because triclosan dissociated at a final solution pH higher than 9, triclosan adsorption drastically decreased at a pH of 5 for the starting solution. With 4 g L^{-1} of KNF-750, triclosan was removed 90% of the time. Triclosan was

adsorbed endothermically, with a 32.8 kJ mol^{-1} enthalpy change. By demonstrating the disappearance of inorganic Cl and the appearance of organic Cl, XPS examination demonstrated that triclosan was adsorbed on the surface of biochar.

Yu *et al.*[108] investigated how to effectively eliminate TCS with activated carbon (AC) made from nylon 6,6 nanofiber and waste coconut (*Cocos nucifera*) pulp. The effects of physico–chemical parameters and features for both nanofiber and AC were investigated. The AC was made by carbonizing discarded coconut pulp under a nitrogen flow for an hour at 300 °C after treatment with zinc chloride. Utilizing an electrospinning apparatus with a high voltage of 26 kV, an injection rate of 0.4 mL h^{-1}, a tip-to-collector distance of 15 cm, and a rotational speed of 1000 rpm, the nylon 6,6 nanofiber [14 wt%] was created. Variables such as pH, adsorbent dosage, contact time, agitation speed, temperature, and initial TCS concentration were investigated. Additionally, a device for testing flat-sheet membranes was used to perform a filtration test at a pressure of 1.0 bar. Three techniques—Fourier transform infrared spectroscopy (FTIR), Brunauer–Emmett–Teller, and field emission scanning electron microscopy (FESEM)—were used to examine the properties of AC and nylon 6,6 nanofiber (BET). According to the research, while the adsorption method using AC can remove 83.3% TCS in 20 minutes, the filtering method using nylon 6,6 can remove 90.2% TCS in 5 minutes. After combining the adsorption and filtering techniques using AC and nylon 6,6 nanofibers, TCS elimination increased to 100% removal in less than 5 minutes. The Freundlich isotherm is used to research isotherms, while the Langmuir isotherm is used for nylon 6,6 nanofiber. While nylon 6,6 and AC both use the pseudo-second-order model for kinetics studies. This research demonstrated that the use of AC combined with nylon 6,6 nanofiber can enhance the elimination of TCS from water.

4.1.8 Lincosamides. To date the use of agriculturally based adsorbent/biochar for the adsorptive removal of lincosamides is limited; hence, more studies on the application of these materials for the removal of lincosamides from wastewater is needed to ensure their efficacy. Recently, Zoroufchi *et al.*[109] explored the efficiency of using microwave-activated canola straw biochar for adsorbing lincomysin. In this study, batch and dynamic adsorption processes were used to examine the dynamics of lincomysin interactions with microwave-activated biochar. The activation of biochar was perfected by adjusting the activation agent molarity, heating time in a microwave, and microwave power. The results showed that the applied activation process was effective in the production of biochar, with a BET surface area of 1452 m^2 g^{-1} under the optimized conditions, and more than 2 m^2 g^{-1} for the raw biomass. Results obtained from the experiment suggested that the main factor affecting the adsorption process was electrostatic interaction. The maximum adsorption capacity was also found to be 190 mg g^{-1}. Thermodynamic studies also showed that lincomycin adsorbed to biochar in a favorable and spontaneous manner. The results showed that microwave pyrolysis can be used to successfully produce a biochar adsorbent that can be used to effectively remove lincomycin from various water matrices.

4.1.9 Reductase inhibitor: trimethoprim. Trimethoprim (TMP) antibiotic has been shown to be potent against bacteria that are liable to cause urinary infections and bronchitis. It has also been used to treat certain side effects, including nausea, stomach upset and diarrhea. TMP has been shown to be one of the most regularly administered antibiotics. Its existence in water bodies and its persistent nature are major causes for concern.[110] Stopping the administration of these antibiotic agents for the treatment of certain diseases would not be feasible due to its high level of potency. This therefore necessitates research into the development of workable techniques in order to get rid of TMP from water bodies using low-cost biomass-based adsorbents.[111]

A study was carried out by Cheng *et al.*,[112] where feather charcoal was utilized for the adsorption of TMP-polluted waste water. The characterization of feather-derived charcoal showed a well-organized microporous adsorbent with a surface area of 805.4 m^2 g^{-1}. Furthermore, 1.36 and 1.76 mmol g^{-1} were the observed acidic and basic functional groups, respectively, on the surface of the charcoal with a recorded pHpzc value of 7.52. The following adsorption parameters were studied: initial concentration, dosage, time, temperature, pH and ionic strength. The findings of the study show that adsorption kinetics is favored by pseudo-second-order kinetics with an R^2 value of 0.9880. The TMP-feather-derived adsorption isotherms for the biosorbent were better explained by the Freundlich isotherm at lower temperature (293 K) with a q_m value of 125 mg g^{-1} and $R^2 = 0.9913$, while the adsorption process was well fitted to the Langmuir isotherm at higher temperature (313 K) with a q_m value of 164 mg g^{-1} at $R^2 = 0.9984$. The adsorption mechanism was observed to be a combination of hydrophobic interactions and ion exchange as well as electrostatic interaction. This study thereby confirmed the suitability of the feather-derived charcoal as a biosorbent for TMP-polluted wastewater.

Furthermore, a novel low-cost magnetic peanut-based adsorbent (MPN-Bet) was synthesized through a copolymerization technique with Fe_3O_4 and betaine.[111] The modification of the peanut husk alters the available MPN-bet adsorption sites, thereby altering the physicochemical properties and thus enhancing the adsorption potential of the MPN-Bet composite. The finding of the study show that MPN-Bet has potential for the sequestration of TMP from its solution. The maximum adsorption capacity of 31.2 ± 3.2 mg g^{-1} with $R^2 = 0.978$ at 293 K show that the uptake of TMP from its solution using MPN-Bet is exothermic in nature. Both physisorption and chemisorption as shown by the kinetic models employed in this study, suggesting that pseudo-first and pseudo-second-order kinetics play active roles in the adsorption process. However, chemisorption was observed to be the dominant adsorption mechanism. An evaluation of the biopotency of MPN-Bet against *E. coli* and *S. aureus* showed that it effectively inhibited the growth of these microorganisms. These properties promote MPN-Bet as a suitable sorbent for wastewater remediation.

Lee and Kam investigated the adsorption characteristics of TMP onto an activated carbon prepared from waste citrus peel.[113] Response surface methodology was adopted to evaluate the influence of adsorption parameters on TMP adsorption. Batch experiments were carried out according to a four-factor Box–Behnken experimental design, which included

concentration, amount of adsorbent, temperature, and pH. The experimental data was observed to be best fitted to the Langmuir isotherm with a recorded q_m value of 144.9 mg g^{-1} at 293 K. The reaction kinetics were best described by the pseudo-second-order reaction kinetic model.

4.1.10 Multiple antibiotic system. Zeng *et al.*[65] examined the adsorptive efficiency and mechanism of biochars prepared at different pyrolytic temperatures (300–700 °C) of rice straw for the removal of doxycycline and ciprofloxacin. The influence of dosage, pH, contact time, temperature and other operating conditions were studied. The BET surface area increased from 3.29 to 20.55 m^2 g^{-1}, and the pore volume and functionality also changed with increasing heating temperature. The adsorption of DOX and CIP was found to increase rapidly with time, attributed to the availability of active sites on the biochar surface. The experimental data obtained at different temperatures were fitted to Langmuir, Temkin, Freundlich and BET models, and the Freundlich model fitted best with a correlation coefficient of 0.98, indicating that the antibiotics were adsorbed on heterogeneous active sites. The optimum adsorption capacity observed from 298 K to 318 K for DOX (170.36–432.90 mg g^{-1}) was greater than that for CIP (48.80–131.58 mg g^{-1}). On the other hand, the kinetic data correlated best to the pseudo-second-order model with R^2 of 0.998 and 0.997 for DOX and CIP, respectively, suggesting chemisorption. From the results, it was observed that the removal efficiency of BC 700 was highest compared to BC 300 and BC 500. Additionally, from the FTIR spectra, it was suggested that the enhanced adsorption capacity of BC 700 may be as a result of oxygen-containing groups; alkoxy, carboxyl, and hydroxyl groups were seen on the BC 700 surface, which formed H-bonding with the functional groups (–OH, $–NH_2$, –COOH) of CIP and DOX. Intra-particle diffusion was also found to be one of the rate-limiting steps in the adsorption process. In the overall result, BC 700 was a promising, cost-effective BCM for the removal of DOX and CIP.[65]

Another study assessed the adsorption capability of three biochars derived from spent coffee grounds, cattle manure, and biosolids on antibiotics, namely, tetracycline (TET), erythromycin (ERY), clarithromycin (CLA), trimethoprim (TMP) and ampicillin (AMP). Biochar dosage of 1 g L^{-1} or 10 g L^{-1} was applied to a spiked mixture of antibiotic mixtures of 100 μg L^{-1} of an aqueous solution in a batch adsorption process. The results showed that at low dosage, more than 70% of the antibiotics were removed by all biochars applied, while at high dosage, rapid adsorption within 5 min of incubation was observed, resulting in complete removal of TET, CLA, ERY, and CLA as well as >85% of AMP and TMP. From the study, it was revealed that the process is pH-dependent. The experimental data fitted well to the Freundlich isotherm model and the suggested mechanisms responsible for the adsorption were π–π electron-donor–acceptor and hydrogen-bonding. The overall result emphasized the possible utilization of the biochar for the decontamination of antibiotics in the water phase.[69]

In another recent study, self-functionalized biochar from corncob was designed using an ultrasonic-assistant fore-modified method to obtain enhanced adsorption of three targets traditional antibiotics, namely: amoxicillin (AMX), tetracycline (TC), and levofloxacin (LE). The adsorbent characterization revealed an ultra-large surface area of 2368 m^2 g^{-1} and greater functionality, which played a vital role in the adsorbent–adsorbate interface interaction. The experimental data obtained from the batch process fitted well with the Freundlich isotherm model (R^2 = 0.99), which indicated chemisorption. This correlated with the kinetics data, which fitted best to Elovich at a temperature ranging from 20–40 °C. An outstanding adsorptive capability of >497 mg g^{-1} was also observed. The thermodynamics parameters of enthalpy (ΔH) and entropy (ΔS) obtained from the studies were positive, while the Gibb's free energy change (ΔG) decreased with increasing temperature. This revealed that the sorption affinity became intense at a higher temperature. The removal efficiencies reached 97.98%, 72.26%, and 96.59% for LE, AMX and TC respectively. It can be inferred from the process that the ultrasonic-assisted method has the potential to develop a more efficient modified BC for pollutant removal in the water layer.[71]

The modification of powdered pistachio shells with ZnO nanoparticles to prepare a viable adsorbent has been exploited to get rid of tetracycline, amoxicillin, and ciprofloxacin antibiotics from aqueous solution.[114] The adsorption isotherm for the removal of tetracycline and ciprofloxacin was best fitted with the Freundlich model, while the Langmuir model best interpreted the removal of amoxicillin. Moreover, the maximum adsorption capacities of 92.450, 98.717 and 132.24 mg g^{-1} were attained for tetracycline, amoxicillin and ciprofloxacin, as deduced from the Langmuir isotherm model. Additionally, the correlation of the pseudo-second-order kinetic data with the removal of the antibiotics implies a chemical adsorption controlled process in a spontaneous and exothermic approach pinpointed in the thermodynamic studies.[114]

The utilization of chemical agents, for instance, HNO_3, NaOH, $ZnCl_2$, KOH, and NaCl, for the modification of vine wood to generate carbon nanoparticles for removing selected antibiotics that include tetracycline, cephalexin, penicillin G and amoxicillin has been reported.[115] From the experimental outcomes, it was pointed out that NaOH-activated adsorbents exhibited the highest removal rate compared to the adsorbents derived from other activating agents at the optimum condition of pH (2), 20 mg L^{-1} (antibiotic concentration), 8 h of contact time and 0.4 g L^{-1} adsorbent dose at 45 °C. Correspondingly, the kinetics studies revealed a pseudo-second-order controlled adsorption process.[115]

5 Adsorption kinetics models: theoretical basis

In past years, different models and mathematical formulas have been used to describe the kinetics[128,129] and mechanisms of adsorption processes,[130] specifically, the equilibrium adsorption proficiency of various solutes. The adsorption mechanism is also affected by the adsorbents' physical properties and chemical attributes.[130] These models include but are not limited to the following models.

5.1 Lagergren pseudo-first-order model

The pseudo-first-order kinetic model is commonly used to explain the adsorption process in relation to boundary

diffusion. It is the most frequently used adsorption model.[131] Lagergren presented a first-order rate equation to describe the kinetic process of liquid–solid phase adsorption. The pseudo-first-order kinetic model is often used for solute adsorption from liquid.[132] It is said to be the first model established on adsorption capacity.[133] It is used to explain the adsorption kinetics of various species. For lower solute concentrations, the pseudo-first-order kinetic model by Lagergren is particularly appropriate.[130] This model has been frequently used in recent years to describe the adsorption of contaminants/pollutants from wastewater in several fields. It has been popularly used in recent years to explain contaminant adsorption from wastewater in a variety of disciplines.[133] It can be expressed as in eqn (1) & (2) in Table 4.

5.2 Lagergren pseudo-second-order model

The Lagergren pseudo-second-order-model approach can be used to determine the rate constants, equilibrium adsorption capacity, and adsorption mechanism of adsorption processes.[129] It can be expressed as eqn (3) in Table 4.

5.3 Intra-particle diffusion model

The intra-particle diffusion model was developed to see whether intra-particle diffusion is the rate-limiting stage in an adsorption process.[134] The intra-particle diffusion model implies that intra-particle diffusion is the only phase affecting the rate[135] and that the membrane diffusion can be ignored.[136] Doğan *et al.* reported in 2009 that the intra-particle diffusion step is most often the rate-limiting step in adsorption processes.[132] It is written as eqn (4) in Table 4.

5.4 Avrami kinetic model

In Avrami's model, adsorption kinetics is an exponential function of adsorption time. The fractional-order kinetic model of Avrami was created to explain phase transition and to evaluate crystal formation in materials.[137] The mole fraction of the gas phase and sorption temperature are relevant considerations when the Avrami model is applied.[131] The Avrami model depends on the overall rate of adsorption and can be used where there is multiple adsorption mechanism. It is written as eqn (5) in Table 4.

5.5 Bangham kinetic model

The Bangham kinetic model has also been used to determine the rate-controlling step of an adsorption process.[138] According to Wang *et al.*,[136] the Bangham adsorption equation can also be written as in eqn (6) and (7).[139]

5.6 Boyd kinetic model

This Boyd kinetic model differentiates the extra particle and intra-particle diffusion.[139] It can be expressed mathematically as represented in eqn (8).

5.7 Elovich kinetic model

Recently, the Elovich equation has been frequently utilized to characterize the kinetics of gas adsorption on solids[140,141] as well as the adsorption of contaminants from aqueous solutions.[139]

Table 4 Adsorption kinetic models[a]

Type	Expression	Equation	Ref.
Lagergren pseudo-first-order	$\log(Q_e - Q_t) = \log Q_e - \frac{k_1 t}{2.303}$	(1)	130, 135 and 143
	$\ln(Q_e - Q_t) = \ln Q_e - k_1 t$	(2)	144
Pseudo-second-order	$\frac{t}{Q_t} = \frac{1}{Q_e} t + \frac{1}{k_2 \cdot {Q_e}^2}$	(3)	144 and 145
Intra-particle diffusion model	$Q_t = k_i t^{\frac{1}{2}} + I$	(4)	146–149
Avrami	$Q_t = Q_{av}(1 - e^{(k_{av} t)^{n_{av}}})$	(5)	131 and 144
	$\ln(-\ln(1 - Q_t)) = \ln(K_{av}) - n_{av} \ln(t)$		
Bangham	$Q_t = Q_e - (Q_e - Q_0)\exp(-k_B t^{\mu})$	(6)	136
	$\log\left(\log\frac{C_t}{C_i} - Q_t m\right) = \log K_0 - Q_t \log(t)$	(7)	139
Boyd	$B_t = -0.4977 - \ln\left(1 - \frac{Q_t}{Q_e}\right)$	(8)	139
Elovich	$Q_t = \frac{1}{\beta}\ln(\alpha\beta) - \frac{1}{\beta}\ln(t)$	(9)	150

[a] Notation: Q_e = adsorption capacity at equilibrium (mg g^{-1}), Q_t = adsorption capacity at time t (mg g^{-1}), k_1 = pseudo-first-order adsorption equilibrium rate constant of (1/min), t = time of contact (min), k_2 = equilibrium rate constant of pseudo-second-order adsorption (g mg^{-1} min^{-1}), k_i = intra-particle diffusion rate constant (mg g^{-1} $min^{-0.5}$), I = constant that gives the information regarding the thickness of the boundary layer (mg g^{-1}), $t^{1/2}$ = half-life, Q_{av} = Avrami theoretical value of the amount of the adsorption (mg g^{-1}), K_{av} = Avrami constant rate, n_{av} = Avrami order model, Q_t = the amount of adsorbate in the adsorbent at time t (mg.g^{-1}), C_t = solution concentration at time t, C_i = adsorbate initial concentration (mg L^{-1}), Q_t = the amount of adsorbate in the adsorbent at time t (mg g^{-1}), m = the mass of the adsorbent in a litre of adsorbate (g L^{-1}), k_B = rate constant for Bangham's model, B_t = Boyd constant, β = the number of sites available for adsorption, α = the initial adsorption rate (mg g^{-1} min).

The Elovich model assumes that the surfaces of solids are actively heterogeneous.[142] It is mathematically expressed as eqn (9) in Table 4.

6 Adsorption isotherm models: theoretical basis

The adsorption capacities of different adsorbents and their relationships with various adsorbates are often expressed using different types of adsorption isotherms. Since a single isotherm model cannot be used to describe an adsorption process in general, we have put together the mathematical expressions for frequently used isotherms in Table 5. Additionally, we summarize the unique features and characteristics of these isotherms in order to provide the theoretical background to which they could be further applied.

The Langmuir isotherm model is one of the most common and simple to use isotherms due to its effectiveness in low concentrations, flexibility with computer simulations, and easy handling.[151] This model works on the principle of homogeneous adsorption and monolayer formation with no interaction between the adsorbed species. It is expressed as eqn (10) and eqn (11)–(14) in non-linear and linear models. Together with the Langmuir isotherm model, the Freundlich isotherm is also commonly used. This model works on the principle of heterogeneity and multilayer adsorption and depends on the concentration of pollutants. The Freundlich model is frequently used because its capacity to describe nonlinear adsorption even in the smallest amount of the adsorbate coped with its functionality in heterogeneous systems, which are common for adsorption. Mathematically, the Freundlich isotherm is expressed as non-linear (eqn (15)) and linear (eqn (16)). Many studies have compared the Bohart–Adams isotherm model with that of the Thomas and Yoon–Nelson models, even though most of these studies present contrary ideas.[152,153] The uniqueness of the Bohart–Adams isotherm is based on its assumption that equilibrium is not instantaneous and the dependence on surface reaction theory. The performance of the Bohart–Adams model can be evaluated using nonlinear (eqn (17)) and linear (eqn (18)) equations.

The Langmuir isotherm model had some barriers and the BET isotherm was developed years later to address these flaws. The BET theory extends the Langmuir theory to multilayer adsorption with additional assumptions that the principle of Langmuir theory can be applied to each layer, that a dynamic equilibrium exists between successive layers, and last that the enthalpy of adsorption of the first layer is constant. This model is expressed as non-linear (eqn (19)) and linear (eqn (20)). Since the Langmuir isotherm is limited to homogeneous surfaces, the Dubinin–Radushkevich isotherm was considered more advanced because it accounts for the effect of the porous structure of the adsorbents.[173] The Dubinin–Radushkevich isotherm assumes that adsorption depends on the filling of the micropore volume, contrary to known layer-by-layer models.[174,175] Since this model has been applied in aqueous solutions, its accuracy depends on the ε values.[176] It can be expressed as non-linear (eqn (21)) and linear (eqn (22)). The Flory–Huggins isotherm believes that the chain elements arrange themselves randomly on a three-dimensional structure. Based on this assumption, the Flory–Huggins isotherm is used to describe the coverage characteristics of the adsorbate. This isotherm is expressed as nonlinear (eqn (23)) and linear forms (eqn (24)).

The Frenkel–Halsey–Hill isotherm basically works on the principle of pair potential that adsorbate particles interact with other particles such as the substrate during adsorption. It assumes that the sum of individual adsorbate–substrate or adsorbate–adsorbate interactions present the total interaction. Mathematically, this isotherm is expressed in a nonlinear (eqn (25)) form. The Khan isotherm is a summed-up model recommended for a pure mixture, which can address the two limits of the Langmuir and Freundlich types. It was created for both multicomponent and single-part adsorption frameworks. Mathematically, this isotherm is expressed in a nonlinear (eqn (26)) form. As a three-parameter equation, the Koble–Corrigan isotherm works on the Langmuir and Freundlich isotherm principle for assessing the equilibrium adsorption of various systems. When the concentration of adsorbate is high, the Koble–Corrigan isotherm conditions itself to the principle of the Freundlich isotherm.[159] Mathematically, this model can be represented as a non-linear equation (eqn (27)) and a linear equation (eqn (28)). The MacMillan–Teller isotherm is an adsorption model deciphered from incorporating surface chemistry in the BET isotherm. This isotherm can be expressed as a non-linear model (eqn (29)).

The Radke–Prausnitz isotherm accepts that an adsorbent should be thermodynamically idle; for instance, its properties (for example, interior energy) do not influence the adsorption process. Mathematically, it is expressed as a non-linear equation (eqn (30)). The Redlich–Peterson isotherm is an experimental model with a consolidated component of both Langmuir and Freundlich isotherms, containing vague three boundaries joining its three conditions. This model can be applied for homogeneous and heterogeneous surfaces, and it does not follow ideal monolayer adsorption; as a result, this model gives the best understanding of trial information. Mathematically, this isotherm can be shown as a non-linear equation (eqn (31)) and linear equation (eqn (32)). The Sips isotherm is a joined type of Langmuir and Freundlich model derived for anticipating the adsorption in heterogeneous frameworks and evading the restriction of the rising adsorbate focus related to the Freundlich isotherm. At low adsorbate fixations, it reduces to the Freundlich isotherm, while at high focus, it predicts monolayer adsorption, like the Langmuir isotherm. Along these lines, the Sips isotherm will be utilized to portray just monolayer adsorption frameworks. It is expressed as a non-linear equation (eqn (33)) and a linear equation (eqn (34)). The Temkin isotherm model assumes that the adsorption heat of all molecules decreases linearly with the increase in coverage of the adsorbent surface and that adsorption is characterized by a uniform distribution of binding energies up to maximum binding energy. It is expressed as a non-linear equation (eqn (35)) and a linear equation (eqn (36)).

Table 5 Mathematical expressions in both nonlinear and linear forms for frequently used isotherms[a]

Isotherm	Nonlinear form	Equation	Linear form	Equation	Plot	Ref.
Langmuir	$Q_e = \frac{K_L Q_L C_e}{1 + K_L C_e}$	(10)	$\frac{C_e}{Q_e} = \frac{1}{K_L Q_L} + \frac{C_e}{Q_L}$	(11)	$\frac{C_e}{Q_e}$ *vs.* C_e	154
			$\frac{1}{Q_e} = \frac{1}{K_L Q_L C_e} + \frac{1}{Q_L}$	(12)	$\frac{1}{Q_e}$ *vs.* $\frac{1}{C_e}$	
			$Q_e = Q_L - \frac{Q_e}{C_e K_L}$	(13)	Q_e *vs.* $\frac{Q_e}{C_e K_L}$	
			$\frac{Q_e}{C_e} = K_L(Q_L - Q_e)$	(14)	$\frac{Q_e}{C_e}$ *vs.* Q_e	
Freundlich	$Q_e = K_F C_e^{1/n}$	(15)	$\mathrm{Ln}(Q_e) = \mathrm{Ln}(K_F) + \frac{1}{n}\mathrm{Ln}(C_e)$	(16)	$\mathrm{Ln}(Q_e)$ *vs.* $\mathrm{Ln}(C_e)$	155
Bohart–Adams	$\frac{C_t}{C_i} = \frac{e^{K_{BA} C_i t}}{e^{K_{BA} N_0 Z/U} - 1 + e^{-K_{BA} C_i t}}$	(17)	$\mathrm{Ln}\left(\frac{C_t}{C_i} - 1\right) = \frac{K_{BA} N Z}{U} - K_{BA} C_i t$	(18)	—	156
Brunauer–Emmett–Teller (BET)	$Q_e = \frac{Q_s C_{BET} C_e}{(C_s - C_e)\left(1 + (C_{BET} - 1)\left(\frac{C_e}{C_s}\right)\right)}$	(19)	$\frac{C_e}{Q_e(C_s - C_e)} = \frac{1}{Q_s C_{BET}} + \frac{(C_{BET} - 1)\left(\frac{C_e}{C_s}\right)}{Q_s C_{BET}}$	(20)	$\frac{C_e}{Q_e(C_s - C_e)}$ *vs.* $\frac{C_e}{C_s}$	157
Dubinin–Radushkevich	$Q_e = Q_{DR} e^{-\beta \varepsilon^2}$	(21)	$\mathrm{Ln}(Q_e) = \mathrm{Ln}(K_{DR} \varepsilon^2)$	(22)	$\mathrm{Ln}(Q_e)$ *vs.* ε^2	158
Flory–Huggins	$\frac{\theta}{C_i} = K_{FH}(1 - \theta)^{n_{FH}}$	(23)	$\log\left(\frac{\theta}{C_i}\right) = \log(K_{FH}) + n_{FH}\log(1 - \theta)$	(24)	$\log\left(\frac{\theta}{C_i}\right)$ *vs.* $\log(1 - \theta)$	159
Frenkel–Halsey–Hill	$\ln\left(\frac{C_e}{Q_e}\right) = \frac{-\alpha}{RT}\left(\frac{Q_s}{Q_e d}\right) r$	(25)	—		—	160
Khan	$Q_e = \frac{Q_s b_k C_e}{(1 + b_k C_e) a_k}$	(26)	—		—	161
Koble–Corrigan	$Q_e = \frac{A(C_e)^n}{1 + B(C_e)^n}$	(27)	$\frac{1}{Q_e} = \frac{1}{A(C_e)^n} + \frac{B}{A}$	(28)	—	162
MacMillan–Teller	$Q_e = Q_s\left(\frac{k}{\ln\frac{C_s}{C_e}}\right)^{\frac{1}{3}}$	(29)	—		—	163
Radke–Prausnitz	$Q_e = \frac{a_{RP} r_R (C_e)^{\beta_R}}{a_{Rp} + r_R (C_e)^{\beta_{R-1}}}$	(30)	—		—	164
Redlich–Peterson	$Q_e = \frac{K_R C_e}{1 + a_R C_e^g}$	(31)	$\ln\left(K_R \frac{C_e}{C_s} - 1\right) = g \ln C_e - \ln a_R$	(32)	—	165
Sips	$Q_e = \frac{K_s C_e^{\beta_s}}{1 + a_s C_e^{\beta_s}}$	(33)	$\beta_s \ln C_e = -\ln\frac{K_s}{Q_e} + \ln a_s$	(34)	$\ln\frac{K_s}{Q_e}$ *vs.* $\ln C_e$	166
Temkin	$Q_e = \frac{RT}{b_T}\ln A_T C_e$	(35)	$Q_e = \frac{RT}{b_T}\ln A_T + \frac{RT}{b_T}\ln C_e$	(36)	Q_e *vs.* $\ln C_e$	167
Toth	$Q_e = \frac{K_T C_e}{(a_T + C_e)^{\frac{1}{t}}}$	(37)	$\ln\left(\frac{Q_e}{K_T}\right) = \ln C_e - \frac{1}{t}\ln(a_T + C_e)$	(38)	$\ln\left(\frac{Q_e}{K_T}\right)$ *vs.* $\ln C_e$	168
Wolborska	$\frac{C_t}{C_i} = e^{\left(\frac{\beta C_i}{N_0} t - \frac{\beta Z}{U}\right)}$	(39)	—		—	169
Yoon–Nelson	$\frac{C_t}{C_i} = \frac{1}{1 + e^{-K_{YN}(t - \tau)}}$	(40)	—		—	170
Harkin–Jura	—		$\frac{1}{Q_e^2} = \frac{B_{HJ}}{A_{HJ}} - \frac{1}{A_{HJ}}\log C_e$	(41)	$\frac{1}{Q_e^2}$ *vs.* $\log C_e$	171

Table 5 (*Contd.*)

Isotherm	Nonlinear form	Equation	Linear form	Equation	Plot	Ref.
Halsey	—		$\mathrm{Ln}(Q_e) = \frac{1}{n_H}\mathrm{Ln}(K_H) - \frac{1}{n_H}\mathrm{Ln}(C_e)$	(42)	$\mathrm{Ln}(Q_e)$ *vs.* $\mathrm{Ln}(C_e)$	Naz *et al.* 2021
Elovich–Larionov	—		$\mathrm{Ln}\frac{Q_e}{C_e} = \mathrm{Ln}(K_E Q_E) - \frac{1}{Q_E}Q_e$	(43)	$n\frac{Q_e}{C_e}$ *vs.* Q_e	172

[a] Notation: Q_L is the maximum monolayer adsorption (mg g^{-1}); K_L is the Langmuir isotherm constant (L mg^{-1}); C_e is the equilibrium concentration (mg L^{-1}); Q_e is the amount of adsorbate in the adsorbent at equilibrium (mg g^{-1}); K_F is the Freundlich isotherm constant (mg g^{-1}) (L g^{-1})^n related to adsorption capacity; n is the adsorption intensity; K_{BA} is the Bohart–Adams rate constant; Z is the total bed depth; C_{BET} is the BET adsorption isotherm relating to the energy of surface interaction (L mg^{-1}); C_s is the adsorbate monolayer saturation concentration (mg L^{-1}); Q_s is the theoretical isotherm saturation capacity (mg g^{-1}); K_{DR} is the Dubinin–Radushkevich isotherm constant (mol^2 kJ^{-2}); Q_{DR} is the theoretical isotherm saturation capacity (mg g^{-1}); C_i is the adsorbate initial concentration (mg L^{-1}); K_{FH} is the Flory–Huggins isotherm equilibrium constant (L g^{-1}); n_{FH} is the Flory–Huggins isotherm model exponent; θ is the degree of surface coverage; d is the interlayer spacing (m); R is the universal gas constant (8.314 J mol^{-1} K^{-1}); r is the inverse power of the distance from the surface; T is the temperature (K); α is the Frenkel–Halsey–Hill isotherm constant (J m^r per mole); a_k is the Khan isotherm model exponent; b_k is the Khan isotherm model constant; A is the Koble–Corrigan isotherm constant (L^n mg^{1-n} g^{-1}); B is the Koble–Corrigan isotherm constant (L mg^{-1})^n; n is the adsorption intensity; a_{Rp} is the Radke–Prausnitz isotherm model constant; r_R is the Radke–Prausnitz isotherm model constant; β_R is the Radke–Prausnitz isotherm model exponent. a_R is the Redlich–Peterson isotherm constant (L mg^{-1}); g is the Redlich–Peterson isotherm exponent; K_R is the Redlich–Peterson isotherm constant (L g^{-1}); a_s is the Sips isotherm model constant (L mg^{-1}); K_s is the Sips isotherm model constant (L g^{-1}); β_s is the Sips isotherm model exponent; A_T is the Temkin isotherm equilibrium binding constant (L g^{-1}); b_T is the Temkin isotherm constant; a_T is the Toth isotherm constant (L mg^{-1}); K_T is the Toth isotherm constant (mg g^{-1}); t is the time; C_t is the solution concentration at the fixed bed outlet at time t; N_0 is the maximum volumetric sorption capacity; U is the linear flow rate; Z is the total bed depth; β is the kinetic coefficient of the external mass transfer; K_{YN} is the Yoon–Nelson rate constant; τ is the time required to reach 50% adsorbate breakthrough (min); A_{HJ} is the Harkin–Jura isotherm constant (slope); B_{HJ} is the Harkin–Jura isotherm constant (intercept); K_H is the Halsey constant (intercept); n_H is the Halsey constant (slope); K_E is the Elovich–Larionov isotherm constant; Q_E is the Elovich–Larionov maximum adsorption capacity (mg g^{-1}).

The Toth isotherm model is another empirical equation developed to improve the Langmuir isotherm model. It is used to describe heterogeneous adsorption systems in both low and high concentrations. It is expressed as a non-linear equation (eqn (37)) and a linear equation (eqn (38)). The Wolborska model depicts the adsorption elements utilizing the mass exchange conditions related to the diffusion means at low levels.[169] It is expressed as a non-linear equation (eqn (39)). The Yoon–Nelson isotherm model described that the pace of decline in the adsorption indicates that the adsorbate particle is relative to the forward leap on the adsorbent.[170] It is expressed as a non-linear equation (eqn (40)). The Harkin–Jura isotherm model assumes the possibility of multilayer adsorption on the adsorbent surface with a heterogeneous pore distribution.[171] Mathematically, this model can be expressed as a linear equation (eqn (41)). The Halsey isotherm is largely applied for multilayer adsorption.[177] It is expressed as a linear equation (eqn (42)). The Elovich–Larionov isotherm portrays the adsorption of non-electrolytes from a solution on a solid surface. It is expressed as a linear equation (eqn (43)).

7 Experimental insight into the application of kinetics and isotherm to antibiotics

7.1 Adsorption kinetics

The adsorption process is an established method extensively researched for how water and wastewater can be remediated. The major methods that are utilized in carrying out adsorption experiments could be either a continuous or a batch process. The latter has been observed to be adopted to a major degree and reported in adsorption experiments due to its lower complexity and the better reliability of its results.[7] This phenomenon (batch or continuous operations) is based on the interaction between the adsorbate and the adsorbent surface through either physical or chemical bonding processes.[178] There are basically four steps that are involved in adsorption kinetics: bulk transport, film transport, intra-particle transport, and adsorption on the adsorbent. The film transport has been reported to be the determinant of the interboundary rate of molecular diffusion and as such regarded as the rate-controlling step of the adsorption process.[67,179]

However, a series of kinetic modeling experiments is carried out to evaluate the rate-controlling steps during the remediation process of an antibiotic or dye polluted wastewater solution by adsorbents (of either chemical or biological source, or a hybrid of both chemical and biological material). The models are categorized into different differential equations, which are basically solved by integral analysis methods.[25] They include zero-order, first-order/pseudo-first-order, second-order/pseudo-second-order, and third-order, which are adopted to provide insight into adsorption kinetics. These kinetic models and their respective parameters, including rate constants, equilibrium adsorption capacities, and related correlation coefficients, are presented in Table 6 to utilize a series of biomass-based sorbents to remove antibiotics from their solution.

Table 6 Adsorption kinetics and isotherm models of selected biomass adsorbent for antibiotic removal[a]

Materials	Antibiotic	Experimental conditions	Adsorption capacity/ removal efficiency	Kinetics	Isotherms	Mechanism	Ref.
Waste tea residue	Hydralazine hydrochloride	IC: 100 mg L^{-1}, AD: 10 mg, *T*: 60 min, pH: 6–8, temp.: nil	131.63 mg g^{-1}	—	Langmuir and Freundlich isotherms, Brunauer–Emmett–Teller (BET)	—	180
Activated carbons from urban wastes (post-consumer plastics), and agro-industrial residues (cork powder and peach stones)	Acetaminophen	IC: 120 mg dm^{-3}, AD: 10 mg, *T*: 5 min–24 h, pH: nil, temp.: 30 °C	267 mg g^{-1}	Pseudo-second-order kinetics	Langmuir and Freundlich isotherms		181
Cocoa shell biomass-based adsorbents	Ibuprofen	IC: 0.5 g L^{-1}, AD: 10 mg, *T*: 5 min–24 h, pH: 2, temp.: 22–50 °C	39 mg g^{-1}		IBP adsorption isotherms		182
Garlic peel	Quinolone	IC: 10 mg L^{-1}, AD: nil, *T*: nil, pH: nil, temp.: 298 K	9.8912 mg g^{-1}	Pseudo-first-order, pseudo-second-order and intraparticle diffusion kinetic models	Langmuir, Freundlich, Temkin and Dubinin–Radushkevich (D-R) models	Hydrogen-bonding	183
Sulfonated sawdust	Tetracycline, sulfamethoxazole and bisphenol A	IC: 20 mL., AD: 10 mg, *T*: nil, pH: 4, temp.: 25 °C, 45 °C and 65 °C	270.53 mg g^{-1}, 295.06 mg g^{-1}, and 263.75 mg g^{-1}	Pseudo-first-order, pseudo-second-order and intra-particle diffusion kinetic models	Langmuir, Freundlich, Temkin and Dubinin–Radushkevich (D–R) isotherm	Physiosorption	96
Arundo donax Linn.	Amoxicillin	IC: 50–450 mg L^{-1}, AD: 0.5 g L^{-1}, *T*: 24 h, pH: 7.0, temp.: 323 K	345.4 mg g^{-1}	Pseudo-first-order, pseudo-second-order and intra-particle diffusion kinetic models	Langmuir, Freundlich and Sips isotherms	Endothermic and physisorption	184
Aminated graphitic carbon derived from corn stover biomass	Tetracycline	pH: 7.4, AD: 0.98 g L^{-1}, IC: 50–200 mg L^{-1}	132.9 mg g^{-1}	Pseudo-first-order, pseudo-second-order and intra-particle diffusion kinetic models	Langmuir, Freundlich, Temkin and Dubinin–Radushkevich (D–R) isotherm		185
Steam-activated biochars of *Sicyos angulatus* L.)	Sulfamethazine	IC: 2.5–50 mg L^{-1}, AD: 1 g L^{-1}, *T*: 72 h, pH: 3, 5, 7 and 9, temp.: 25 °C	37.7 mg g^{-1}		Langmuir, Freundlich, Temkin, and Dubinin–Radushkevich (D–R)	Chemisorption and electrostatic interactions	186
NaOH-activated macadamia nut shells	Tetracycline	IC: 500.0, 550.0 and 600.0 mg L^{-1}, AD: 25 mg, *T*: 2.5–180 min, pH: 3–10, temp.: nil	455.33 mg g^{-1}	Pseudo-first-order, pseudo-second-order, Elovich, and Avrami	Langmuir, Freundlich, and Temkin	Intraparticle diffusion and film diffusion	187
High surface area-activated carbons based on olive biomass	Amoxicillin	IC: 100–1400 mg L^{-1}, AD: 30 mg, *T*: 1 to 360 min, pH: 7, temp.: 25 °C	237.02 mg g^{-1}	Pseudo-first-order, pseudo-second order, and Avrami fractional-order	Langmuir, Freundlich and Liu	π–π stacking (π bonds of the drug molecules with π bonds of adsorbent	188

Table 6 (*Contd.*)

Materials	Antibiotic	Experimental conditions	Adsorption capacity/ removal efficiency	Kinetics	Isotherms	Mechanism	Ref.
Non-living *Chlorella* sp.	Cephalexin	IC: 482.92 mg L^{-1}, AD: 50 mg, *T*: 15–600 min, pH: , temp.: 27 °C	129.87 mg g^{-1}		Freundlich and Langmuir isotherms		189
Pseudomonas putida	Ceftriaxone	IC: 15, 10, 20, and 50 mg L^{-1}, AD: 0.1 g, *T*: 6, 12, 24, 48, and 72 h, pH: 7, temp.: 25, 35, and 42 °C	109.5 mg g^{-1}		Freundlich and Langmuir isotherms		190
Rhizopus oryzae biomass	Tetracycline	IC: 10–200 mg L^{-1}, AD: 0.25–5 g L^{-1}, *T*: 5–200 min, pH: 2–11, temp.: 25–50 °C	67.93 mg g^{-1}	Pseudo-first-order, pseudo-second-order, and Elovich	Langmuir, Freundlich and Dubinin–Radushkevich (D–R)	π–π or cation–π interaction	191
Bentonite, activated carbon, zeolite, and pumice	Ciprofloxacin	IC: 20, 25, 30, and 40 mg L^{-1}, AD: 0.0125 g, *T*: 5, 10, 20, 30, 40, 50, and 60 min, pH: nil, temp.: 22 °C	91, 87, and 51% for bentonite, activated carbon, and zeolite, respectively	Pseudo-first, pseudo-second, Elovich equations, and intraparticle diffusion		π–π interaction	192
Super-magnetization of pectin from orange-peel biomass	Sulfamethoxazole	IC: 200 ppm, AD: 1 g, *T*: 24 h, pH: 3–8, temp.: 15, 25, 35 and 45 °C	120 mg L^{-1}	Pseudo-first, pseudo-second-order	Langmuir, Freundlich, and Redlich–Peterson	Electrostatic-interactions	193
Vine wood	Amoxicillin, cephalexin, tetracycline and penicillin G	IC: 20, 30, 50, 80, 100, 150 and 200 mg L^{-1}, AD: 0.05, 0.1, 0.2, 0.3, 0.4, 0.5 and 0.6 g L^{-1}, *T*: 120, 240, 360, 480, 600, 720 and 840 min, pH: 1–12, temp.: 35, 45 and 55 °C	Amoxicillin (2.69 mg g^{-1}), cephalexin (7.08 mg g^{-1}), tetracycline (1.98 mg g^{-1}), penicillin G (8.41 mg g^{-1})	Pseudo-first, pseudo-second and intraparticle diffusion	Langmuir and Freundlich isotherms	Protonation, hydrogen bonding or van der Waals forces	194
Lignin-derived biomass	Tetracycline	IC: 1–300 mg L^{-1}, AD: 15 mg, *T*: 1–120 min, pH: nil, temp.: 298, 308, and 318 K	173.9 mg g^{-1}	Pseudo-first-order, pseudo-second-order, intra-particle diffusion, Elovich	Langmuir, Freundlich, and Dubinin–Radushkevich isotherms	Chemisorption and intraparticle diffusion	195
Amino-functionalized biomass-derived porous carbons	Sulfonamide	IC: 1–20 mg L^{-1}, AD: 5.0 mg, *T*: 720 min, pH: nil, temp.: 25 °C	124.6 mg g^{-1}	Pseudo-second-order	Langmuir and Freundlich isotherms	Electron donor–acceptor interaction	196

Table 6 (*Contd.*)

Materials	Antibiotic	Experimental conditions	Adsorption capacity/ removal efficiency	Kinetics	Isotherms	Mechanism	Ref.
Tea waste biochar	Sulfamethazine	IC: 0–50 mg L^{-1}, AD: 1 g L^{-1}, *T*: 72 h, pH: 3, 7, 9 and 10, temp.: 25 °C	33.81 mg		Freundlich and Langmuir isotherms	π–π electron donor–acceptor interaction, cation–π interaction and cation exchange	186
Grape stalk	Ofloxacin and chrysoidine	IC: 3.1 mM or 7.0 mM, AD: 0.5 g, *T*: 120 min, pH: 4, 7 and 9	137.3 mg g^{-1}	Pseudo-second-order	Langmuir isotherm	π–π interaction	197

[a] IC: initial concentration, AD: adsorbent dose, *T*: time and temp.: temperature (°C/K).

7.2 Adsorption isotherm

Adsorption isotherms represent the relationship between the adsorbate concentration in the adsorbent phase and determine the amount of dissolved concentration at equilibrium.[67] This simply shows that isotherms are used to predict the adsorption capacity of an adsorbent effectively, that is, the amounts of solutes the sorbent can adsorb on its surface per time.[7] Furthermore, the isotherms have the tendency to show the distribution ratio of the antibiotics on the adsorbent's surface at various equilibrium concentrations. There are several adsorption isotherm models; including the Langmuir, Freundlich, Brunauer–Emmett–Teller (BET), Temkin, Frumkin, Harkins–Jura, Smith, and Dubinin–Radushkevich (D–R) isotherms. The Langmuir model shows that once the available adsorptive site is filled, which is termed monolayer covering *via* homogeneous energy distribution, the adsorption process is terminated. The Freundlich isotherm is suitable for the heterogeneous surface adsorption process; there is a tendency for more adsorption to occur even when the monolayer surface is covered.[7,37] While the D–R isotherm model is a combination of both Freundlich and D–R isotherms, it accommodates the adsorption of antibiotics at low concentrations onto both homogeneous and heterogeneous surfaces. It helps determine the mechanism of the adsorption processes: either physisorption or chemisorption.[67] The earlier studies have reported different adsorption isotherm and antibiotics kinetics, as presented in Table 6.

8 Regeneration of adsorbents

The process of regenerating biomass-based adsorbents is termed the inverse of the adsorption process. Two principles are involved in the regeneration of adsorbents: adsorbate decomposition and adsorbate desorption.[198] A high-quality adsorbent should have good recycling and reusable abilities for industrial purposes and very good regenerative ability, which reduces adsorbent costs.[199,200] Magnetic biochar adsorbent regeneration prepared with the eucalyptus leaf residue used in the tetracycline adsorption revealed no significant band shifts in Fourier transform infrared spectra. Furthermore, there was no significant difference in the functional groups present on the regenerated adsorbent while the ash content slightly increased. Thermal and solvent regeneration techniques can be adapted to regenerate biomass used in the adsorption of antibiotic pollutants.

8.1 Thermal regeneration

One effective means of achieving desorption is through thermal regeneration. It involves the decomposition of carbonized adsorbate at high temperature, thus making its molecules smaller than the pore size of biochar adsorbent, thus making desorption occur.[201] It has been established that regeneration efficiency increases with increasing pyrolysis temperature. Regenerated biochar made from *Enteromorpha prolifera* at 80 °C, 150 °C, and 200 °C retained pyrene uptake of 35.00%, 45.00%, and 48.00% while the rates of regeneration of benzo[*a*]pyrene were 31.00%, 41.00%, and 40.00%, respectively.[202]

Removal of dissolved organic carbon can be effectively carried out using thermal treatment.[203]

8.2 Solvent regeneration

Regeneration of solvent uses an equilibrium relationship among biomass, adsorbate, and solvent to break the equilibrium set up in the adsorption process by altering the pH value and temperature of the solvent in order to desorb the adsorbate from activated carbon.[204] Solvent regeneration is a good technique for organic matter adsorbents with low boiling points and high concentrations.[205] Solvent regeneration can be achieved by using inorganic chemicals such as inorganic acids like hydrochloric acid or soluble bases such as sodium hydroxide and other reagents for adsorbate removal, termed the acid–base regeneration technique or through the use of organic solvent. Organic solvent regeneration involves the extraction of adsorbed adsorbents on activated carbon from organic solvents such as methanol, benzene, or acetone. The adsorption involves the principle of integration and similarity.[206]

9 Potential application of the adsorbents in engineering

The use of a biomass-based adsorbent for the construction of fixed beds helps remove organic substances in water and is usually employed to treat contaminated water.[207] The most recent adsorber in a fixed bed for water treatment is constructed such that it can either be an open gravity filter or a closed pressure filter. Concrete or steel that is resistant to corrosion is often employed as a filter material. The most common arrangement of a fixed bed is to fill the inlet with a certain amount of biomass-based adsorbent with very high adsorption capacity, and the outlet also has a certain amount of adsorbent to reduce bed resistance and improve the bed resistance efficiency of mass transfer.[208] A small sand bed is placed between the bottom end of the fixed bed and the activated carbon to get rid of the toner, as shown in Fig. 4. Using a fixed bed, the wastewater treatment plant process can be made continuous by placing multiple adsorbers in series, thus minimizing capacity loss. Two possible ways of connecting multiple adsorbers to a single fixed bed exist: series and parallel. The process involves dividing the total mass of the adsorbent into four parts, with three being used for treatment while the fourth adsorbent is used for regeneration. The time it takes for the first adsorber to be inactive and the mass transfer zone (MTZ) between the third and fourth adsorbers is termed t_1. After a while, the adsorbent present in the second adsorber becomes completely saturated at equilibrium and the MTZ therefore leaves the second adsorber. The time at which this process occur is denoted t_2. The processes continue to obtain t_3 and t_4. Ideally, the adsorbent bed continues to operate until the equilibrium load is attained and this involves continuous operation of the four adsorbers. Different adsorbers are used at various starting times.

The advantage of parallel connections in fixed beds is that the total cross-sectional area increases with an increasing number of adsorbers. Therefore, this means that the multi-adsorber system can be adjusted based on the requirements of the water to be treated. A large amount of water to be treated can be suitably handled by this fixed bed. Factors such as humidity, gas velocity, temperature, side stream effect, pressure drop, and other factors affect the efficiency of the fixed bed in water treatment.

10 Concluding remarks and future perspectives

The global production of a high volume of agricultural wastes without conversion to sustainable products has been attributed to the cause of rural environmental pollution and to a certain degree, increasing the burden of rural agricultural production. By extension, the increase in sustainable products obtained from agricultural wastes can be used to effectively decrease the level of air pollution resulting from the incineration of agricultural wastes. Constructively, the production of biomass-based adsorbents has been postulated to play essential roles in water treatment operations, climate change, and environmental protection in general. Furthermore, global reports on the modification of biomass-based adsorbents for enhancing their adsorption capacities have received tremendous attention and encouragement. This has resulted in the drive for modifying agents that can further increase the adsorption capacity of biomass-based adsorbents. Conversely, attention has recently been drawn to the environmental problems connected with some chemical modifying agents as well as the cost implications and intricacy involved in the modification process. The deployment of agricultural wastes for bio-carbon is posited as

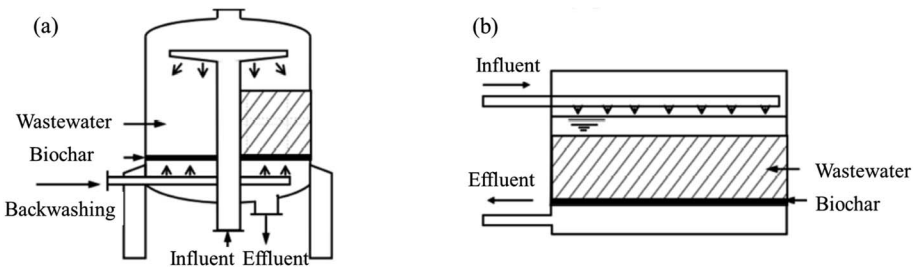

Fig. 4 Typical water treatment fixed-bed adsorbents: (a) corrosion-resistant pressure GAC filter made of steel and (b) rectangular gravity concrete filter.[209]

the core universal competitive approach of green and sustainable technology. The spotlight is presently on carbon sequestration, resource cycling, energy saving, environmental waste management, emission reduction, and tackling the issue of climate change. Consequently, the future of biomass-based adsorbents should be organized according to the following perspective:

(1) Technology for agricultural waste carbonization should be explored and advanced in order to promote the industrial development of biomass-based adsorbents.

(2) Highly efficient green modifying agents and modification processes should be developed that will be employed in the biological sorption process.

(3) Prospective research should be extended to the exploitation of biomass-based adsorbents in dealing with the engineering glitches of pollution scaling.

(4) Due to their merits allied with biomass-based adsorbents, agricultural wastes can be used in substituting for pricey commercial activated carbon for application in environmental protection.

(5) Unfortunately, there is little discussion on handling used adsorbents/biosorbents and sequestered antibiotics. As a result, it is unclear what happened to the residual solutions and the utilized sorbents (and where they were discharged) at the end of the experiments. This would also assist in determining whether or not such successful experiments and inquiries also constitute a risk to the environment.

(6) The majority of the literature reviews were conducted in a synthetic aqueous environment, which might restrict the potential of sorption processes owing to matrix effect(s) that can interfere with sorption in real-world practical systems. As a result, real-world applications and thorough assessments of potential impact interference on the sorption processes are necessary.

(7) To date, there has been only a little research on the use of machine learning to predict antibiotic adsorption onto various adsorbents/biosorbents. As a result, we propose using machine learning to estimate sorption capabilities/efficiencies in water/wastewater.

(8) We also propose employing the partition coefficient (PC) approach to conduct the ideal sorbent assessments, as this will aid in assessing the adsorbents' performance metrics in real applications. In a solid–liquid system, PC is defined as the ratio of q_{max} to equilibrium concentrations. Some biosorbents/adsorbents that have been found to be effective, based on q_{max} studies, may have decreased adsorption capacity in an ambient setting. As a result, performance metrics utilizing the PC approach are able to provide better assessments of the sorption capacities of different sorbents. This could also be used for comparing the effectiveness of these biosorbents/adsorbents.

Data availability

All data and materials used in this study are available within this article.

Author contributions

All authors contributed equally.

Conflicts of interest

The authors declare no conflict of interest.

Acknowledgements

The authors acknowledge their respective Universities for the platform to carry out this study. O. S. Bello acknowledges the support obtained from LAUTECH 2016 TET Fund Institution Based Research Intervention (TETFUND/DESS/UNI/OGBOMOSO/RP/VOL. IX).

References

1 D. Mangla, A. S. Annu and S. Ikram, *J. Hazard. Mater.*, 2022, **425**, 127946.
2 Z. Fang, J. Chen, X. Qiu, X. Qiu, W. Cheng and L. Zhu, *Desalination*, 2011, **268**, 60–67.
3 S. I. Polianciuc, A. E. Gurzău, B. Kiss, M. G. Stefan and F. Loghin, *Med. Pharm. Rep.*, 2020, **93**, 231–240.
4 L. Karthik, G. Kumar, T. Keswani, A. Bhattacharyya, S. Sarath Chandar and K. V. Bhaskara Rao, *PLoS One*, 2014, **9**(3), 1–13.
5 A. Gulkowska, H. W. Leung, M. K. So, S. Taniyasu, N. Yamashita, L. W. Y. Yeung, B. J. Richardson, A. P. Lei, J. P. Giesy and P. K. S. Lam, *Water Res.*, 2008, **42**, 395–403.
6 K. A. Adegoke, O. O. Adesina, O. A. Okon-Akan, O. R. Adegoke, A. B. Olabintan, O. A. Ajala, H. Olagoke, N. W. Maxakato and O. S. Bello, *Curr. Res. Green Sustainable Chem.*, 2022, **5**, 100274.
7 K. A. Adegoke, A. O. Olagunju, T. C. Alagbada, O. C. Alao, M. O. Adesina, I. C. Afolabi, R. O. Adegoke and O. S. Bello, *Water, Air, Soil Pollut.*, 2022, **233**, 38.
8 A. O. Ibrahim, K. A. Adegoke, R. O. Adegoke, Y. A. AbdulWahab, V. B. Oyelami and M. O. Adesina, *J. Mol. Liq.*, 2021, **333**, 115593.
9 A. R. Mahmood, H. H. Al-Haideri and F. M. Hassan, *Adv. Public Health.*, 2019, 1–10.
10 T. Schwartz, W. Kohnen, B. Jansen and U. Obst, *FEMS Microbiol. Ecol.*, 2003, **43**, 325–335.
11 S. B. Levy and M. Bonnie, *Nat. Med.*, 2004, **10**, S122–S129.
12 A. Cassini, L. D. Högberg, D. Plachouras, A. Quattrocchi, A. Hoxha, G. S. Simonsen, M. Colomb-Cotinat, M. E. Kretzschmar, B. Devleesschauwer, M. Cecchini, D. A. Ouakrim, T. C. Oliveira, M. J. Struelens, C. Suetens, D. L. Monnet, R. Strauss, K. Mertens, T. Struyf, B. Catry, K. Latour, I. N. Ivanov, E. G. Dobreva, A. Tambic Andraševic, S. Soprek, A. Budimir, N. Paphitou, H. Žemlicková, S. Schytte Olsen, U. Wolff Sönksen, P. Märtin, M. Ivanova, O. Lyytikäinen, J. Jalava, B. Coignard, T. Eckmanns, M. Abu Sin, S. Haller, G. L. Daikos, A. Gikas, S. Tsiodras, F. Kontopidou, Á. Tóth, Á. Hajdu, Ó. Guólaugsson, K. G. Kristinsson,

S. Murchan, K. Burns, P. Pezzotti, C. Gagliotti, U. Dumpis, A. Liuimiene, M. Perrin, M. A. Borg, S. C. de Greeff, J. C. Monen, M. B. Koek, P. Elstrøm, D. Zabicka, A. Deptula, W. Hryniewicz, M. Caniça, P. J. Nogueira, P. A. Fernandes, V. Manageiro, G. A. Popescu, R. I. Serban, E. Schréterová, S. Litvová, M. Štefkovicová, J. Kolman, I. Klavs, A. Korošec, B. Aracil, A. Asensio, M. Pérez-Vázquez, H. Billström, S. Larsson, J. S. Reilly, A. Johnson and S. Hopkins, *Lancet Infect. Dis.*, 2019, **19**, 56–66.

13 C. Bouki, D. Venieri and E. Diamadopoulos, *Ecotoxicol. Environ. Saf.*, 2013, **91**, 1–9.

14 B. Li and T. Zhang, *Environ. Sci. Technol.*, 2010, **44**, 3468–3473.

15 A. S. Oberoi, Y. Jia, H. Zhang, S. K. Khanal and H. Lu, *Environ. Sci. Technol.*, 2019, **53**, 7234–7264.

16 M. Kumar, S. Jaiswal, K. K. Sodhi, P. Shree, D. K. Singh, P. K. Agrawal and P. Shukla, *Environ. Int.*, 2019, **124**, 448–461.

17 K. J. Choi, S. G. Kim and S. H. Kim, *J. Hazard. Mater.*, 2008, **151**, 38–43.

18 V. Diwan, A. J. Tamhankar, M. Aggarwal, S. Sen, R. K. Khandal and C. S. Lundborg, *Curr. Sci.*, 2009, **97**, 1752–1755.

19 M. Malakootian, A. Nasiri and H. Mahdizadeh, *Water Sci. Technol.*, 2018, **78**, 2158–2170.

20 K. D. Burch, B. Han, J. Pichtel and T. Zubkov, *Environ. Sci. Pollut. Res.*, 2019, **26**, 6301–6310.

21 S. Sharma and A. Bhattacharya, *Appl. Water Sci.*, 2017, **7**, 1043–1067.

22 S. M. Ebrahimi, R. D. Reyhani, M. Asghari-JafarAbadi and Z. Fathifar, *Environ. Evid.*, 2020, **9**, 1–9.

23 J. R. De Andrade, M. F. Oliveira, M. G. C. Da Silva and M. G. A. Vieira, *Ind. Eng. Chem. Res.*, 2018, **57**, 3103–3127.

24 D. Dolar, T. I. Zokić, K. Košutić, D. Ašperger and D. M. Pavlović, *Environ. Sci. Pollut. Res.*, 2012, **19**, 1033–1042.

25 M. B. Ahmed, J. L. Zhou, H. H. Ngo and W. Guo, *Sci. Total Environ.*, 2015, **532**, 112–126.

26 A. Choudhry, A. Sharma, T. A. Khan and S. A. Chaudhry, *J. Water Process. Eng.*, 2021, **42**, 102150.

27 S. Purnell, J. Ebdon, A. Buck, M. Tupper and H. Taylor, *Water Res.*, 2015, **73**, 109–117.

28 C. A. Quist-Jensen, F. Macedonio and E. Drioli, *Desalination*, 2015, **364**, 17–32.

29 H. Rondon, W. El-Cheikh, I. A. R. Boluarte, C. Y. Chang, S. Bagshaw, L. Farago, V. Jegatheesan and L. Shu, *Bioresour. Technol.*, 2015, **183**, 78–85.

30 Y. Ben, C. Fu, M. Hu, L. Liu, M. H. Wong and C. Zheng, *Environ. Res.*, 2019, **169**, 483–493.

31 K. Kümmerer, *J. Antimicrob. Chemother.*, 2003, **52**, 5–7.

32 A. J. Ebele, M. Abou-Elwafa Abdallah and S. Harrad, *Emerging Contam.*, 2017, **3**, 1–16.

33 P. Krasucka, B. Pan, Y. Sik Ok, D. Mohan, B. Sarkar and P. Oleszczuk, *Chem. Eng. J.*, 2021, **405**, 126926.

34 H. Shi, J. Ni, T. Zheng, X. Wang, C. Wu and Q. Wang, *Environ. Chem. Lett.*, 2020, **18**, 345–360.

35 F. Mansour, M. Al-Hindi, R. Yahfoufi, G. M. Ayoub and M. N. Ahmad, *Rev. Environ. Sci. Biotechnol.*, 2018, **17**, 109–145.

36 M. Östman, B. Björlenius, J. Fick and M. Tysklind, *Sci. Total Environ.*, 2019, **649**, 1117–1123.

37 K. A. Adegoke and O. S. Bello, *Water Resour. Ind.*, 2015, **12**, 8–24.

38 X. Xie, Z. Zhang, Y. Hu and H. Cheng, *Chem. Eng. J.*, 2018, **334**, 1242–1251.

39 I. Arslan-Alaton and S. Dogruel, *J. Hazard. Mater.*, 2004, **112**, 105–113.

40 J. Peng, X. Wang, F. Yin and G. Xu, *Sci. Total Environ.*, 2019, **650**, 2437–2445.

41 S. F. Yang, C. F. Lin, A. Yu-Chen Lin and P. K. Andy Hong, *Water Res.*, 2011, **45**, 3389–3397.

42 Y. Feng, L. Yang, J. Liu and B. E. Logan, *Environ. Sci.: Water Res. Technol.*, 2016, **2**, 800–831.

43 M. Eddy, *Wastewater Engineering: Treatment and Reuse*, 4th edn, 2004.

44 A. R. Mareddy, *Impacts on water environment*, 2017.

45 P. Zhou, C. Su, B. Li and Y. Qian, *J. Environ. Eng.*, 2006, **132**, 129–136.

46 D. T. Sponza and P. Demirden, *Sep. Purif. Technol.*, 2007, **56**, 108–117.

47 M. C. M. van Loosdrecht, D. Eikelboom, A. Gjaltema, A. Mulder, L. Tijhuis and J. J. Heijnen, *Water Sci. Technol.*, 1995, **32**, 35–43.

48 C. Adams, Y. Wang, K. Loftin and M. Meyer, *J. Environ. Eng.*, 2002, **128**, 253–260.

49 H. Chen, B. Gao and H. Li, *J. Hazard. Mater.*, 2015, **282**, 201–207.

50 A. O. Ifebajo, A. A. Oladipo and M. Gazi, *Environ. Chem. Lett.*, 2019, **17**, 487–494.

51 A. Alahabadi, A. Hosseini-Bandegharaei, G. Moussavi, B. Amin, A. Rastegar, H. Karimi-Sani, M. Fattahi and M. Miri, *J. Mol. Liq.*, 2017, **232**, 367–381.

52 Y. Liu, X. Liu, W. Dong, L. Zhang, Q. Kong and W. Wang, *Sci. Rep.*, 2017, **7**(1), 12437.

53 F. Chen, Q. Yang, J. Sun, F. Yao, S. Wang, Y. Wang, X. Wang, X. Li, C. Niu, D. Wang and G. Zeng, *ACS Appl. Mater. Interfaces*, 2016, **8**, 32887–32900.

54 J. Di, J. Xia, M. Ji, B. Wang, S. Yin, Q. Zhang, Z. Chen and H. Li, *Appl. Catal., B*, 2016, **183**, 254–262.

55 M. M. Huber, S. Canonica, G. Y. Park and U. Von Gunten, *Environ. Sci. Technol.*, 2003, **37**, 1016–1024.

56 E. Adamek, W. Baran and A. Sobczak, *J. Hazard. Mater.*, 2016, **313**, 147–158.

57 Y. Xia and Q. Dai, *Chemosphere*, 2018, **205**, 215–222.

58 S. Chelliapan, T. Wilby and P. J. Sallis, *Water Res.*, 2006, **40**, 507–516.

59 I. Değirmentaş and N. Deveci, *J. Biochem.*, 2004, **136**, 177–182.

60 S. Kim, P. Eichhorn, J. N. Jensen, A. S. Weber and D. S. Aga, *Environ. Sci. Technol.*, 2005, **39**, 5816–5823.

61 C. Zwiener and F. H. Frimmel, *Sci. Total Environ.*, 2003, **309**, 201–211.

62 W. L. Ma, R. Qi, Y. Zhang, J. Wang, C. Z. Liang and M. Yang, *Biochem. Eng. J.*, 2009, **45**, 30–34.
63 Y. Zhou, X. Liu, Y. Xiang, P. Wang, J. Zhang, F. Zhang, J. Wei, L. Luo, M. Lei and L. Tang, *Bioresour. Technol.*, 2017, **245**, 266–273.
64 Y. Xiang, Z. Xu, Y. Wei, Y. Zhou, X. Yang, Y. Yang, J. Yang, J. Zhang, L. Luo and Z. Zhou, *J. Environ. Manage.*, 2019, **237**, 128–138.
65 Z. W. Zeng, X. F. Tan, Y. G. Liu, S. R. Tian, G. M. Zeng, L. H. Jiang, S. B. Liu, J. Li, N. Liu and Z. H. Yin, *Front. Chem.*, 2018, **6**, 1–11.
66 J. Bedia, M. Peñas-Garzón, A. Gómez-Avilés, J. Rodriguez and C. Belver, *Chem. Eng. J.*, 2018, **333**, 58–65.
67 J. O. Eniola, R. Kumar and M. A. Barakat, *Environ. Sci. Pollut. Res.*, 2019, **26**, 34775–34788.
68 H. M. Jang and E. Kan, *Bioresour. Technol.*, 2019, **274**, 162–172.
69 M. Stylianou, A. Christou, C. Michael, A. Agapiou, P. Papanastasiou and D. Fatta-Kassinos, *J. Environ. Chem. Eng.*, 2021, **9**, 105868.
70 X. R. Jing, Y. Y. Wang, W. J. Liu, Y. K. Wang and H. Jiang, *Chem. Eng. J.*, 2014, **248**, 168–174.
71 H. Li, J. Hu, L. Yao, Q. Shen, L. An and X. Wang, *J. Hazard. Mater.*, 2020, **390**, 122127.
72 H. Wang, X. Lou, Q. Hu and T. Sun, *J. Mol. Liq.*, 2021, **325**, 2–10.
73 H. M. Jang, S. Yoo, Y. K. Choi, S. Park and E. Kan, *Bioresour. Technol.*, 2018, **259**, 24–31.
74 L. ling Yu, W. Cao, S. chuan Wu, C. Yang and J. hua Cheng, *Ecotoxicol. Environ. Saf.*, 2018, **164**, 289–296.
75 R. Cela-Dablanca, C. Nebot, L. R. López, D. Fernández-Calviño, M. Arias-Estévez, A. Núñez-Delgado, M. J. Fernández-Sanjurjo and E. Álvarez-Rodríguez, *Processes*, 2021, **9**, 1–12.
76 D. Naghipour, A. Amouei, K. T. Ghasemi and K. Taghavi, *Desalin. Water Treat.*, 2020, **201**, 219–227.
77 D. Balarak, A. Joghatayi, F. K. Mostafapour and H. Azarpira, *Int. J. Life Sci. Pharma Res.*, 2017, **7**, 1–8.
78 H. Mansouri, R. J. Carmona, A. Gomis-Berenguer, S. Souissi-Najar, A. Ouederni and C. O. Ania, *J. Colloid Interface Sci.*, 2015, **449**, 252–260.
79 G. Moussavi, A. Alahabadi, K. Yaghmaeian and M. Eskandari, *Chem. Eng. J.*, 2013, **217**, 119–128.
80 N. Sunsandee, P. Ramakul, S. Phatanasri and U. Pancharoen, *Biotechnol. Rep.*, 2020, **27**, e00488.
81 D. Balarak and K. Chandrika, *Int. J. Pharm. Invest.*, 2019, **9**, 117–121.
82 S. K. Bajpai, M. Bajpai and N. Rai, *Water SA*, 2012, **38**, 673–682.
83 F. Wang, B. Yang, H. Wang, Q. Song, F. Tan and Y. Cao, *J. Mol. Liq.*, 2016, **222**, 188–194.
84 İ. Alacabey, *Molecules*, 2022, **27**, 1380.
85 T. U. T. Dao, H. T. T. Nguyen, D. T. C. Nguyen, H. T. N. Le, H. T. T. Nguyen, S. T. Do, H. H. Loc, T. T. Nguyen, T. D. Nguyen and L. G. Bach, *Cellul. Chem. Technol.*, 2020, **54**, 811–819.
86 M. Elhag Elhussien, *Adv. Biochem.*, 2017, **5**, 89.
87 A. Zhou, Y. Zhang, R. Li, X. Su and L. Zhang, *Desalin. Water Treat.*, 2016, **57**, 388–397.
88 M. C. Tonucci, L. V. A. Gurgel and S. F. de Aquino, *Ind. Crops Prod.*, 2015, **74**, 111–121.
89 D. Balarak and F. Mostafapour, *Br. J. Pharm. Res.*, 2016, **13**, 1–14.
90 L. Kurup, *Water Sci. Technol.*, 2012, **65**, 1531–1539.
91 A. Ashiq, N. M. Adassooriya, B. Sarkar, A. U. Rajapaksha, Y. S. Ok and M. Vithanage, *J. Environ. Manage.*, 2019, **236**, 428–435.
92 A. R. Olivera, Biosorption of pharmaceuticals from wastewater using *Moringa oleífera* as biosorbent, Master of double diploma with the National University of Missions, Engenharia Química, ESTiG – Dissertações de Mestrado Alunos, 2020.
93 Y. Dai, Q. Sun, W. Wang, L. Lu, M. Liu, J. Li, S. Yang, Y. Sun, K. Zhang, J. Xu, W. Zheng, Z. Hu, Y. Yang, Y. Gao, Y. Chen, X. Zhang, F. Gao and Y. Zhang, *Chemosphere*, 2018, **211**, 235–253.
94 H. T. Fan, L. Q. Shi, H. Shen, X. Chen and K. P. Xie, *RSC Adv.*, 2016, **6**, 109983–109991.
95 H. Alidadi, M. Dolatabadi, M. Davoudi, F. Barjasteh-Askari, F. Jamali-Behnam and A. Hosseinzadeh, *Process Saf. Environ. Prot.*, 2018, **117**, 51–60.
96 M. A. Ahsan, M. T. Islam, C. Hernandez, E. Castro, S. K. Katla, H. Kim, Y. Lin, M. L. Curry, J. Gardea-Torresdey and J. C. Noveron, *J. Environ. Chem. Eng.*, 2018, **6**, 4329–4338.
97 W. Stuart, L. Shearer, S. Pap and S. W. Gibb, *J. Environ. Chem. Eng.*, 2022, **10**, 108106.
98 M. C. Ndoun, H. A. Elliott, H. E. Preisendanz, C. F. Williams, A. Knopf and J. E. Watson, *Biochar*, 2021, **3**, 89–104.
99 K. Herrera, L. F. Morales, N. A. Tarazona, R. Aguado and J. F. Saldarriaga, *ACS Omega*, 2022, **7**, 7625–7637.
100 C. C. O. Alves, A. S. Franca and L. S. Oliveira, *BioMed Res. Int.*, 2013, **2013**, 978256.
101 D. Balarak, A. H. Mahvi, S. Shahbaksh, M. A. Wahab and A. Abdala, *Nanomaterials*, 2021, **11**, 3281.
102 W. Xing, Q. Liu, J. Wang, S. Xia, L. Ma, R. Lu, Y. Zhang, Y. Huang and G. Wu, *Nanomaterials*, 2021, **11**, 2950.
103 A. Chen, J. Pang, X. Wei, B. Chen and Y. Xie, *Environ. Sci. Pollut. Res.*, 2021, **28**, 27398–27410.
104 R. Chitongo, B. O. Opeolu and O. S. Olatunji, *Clean: Soil, Air, Water*, 2018, **47**, 1800077.
105 J. Yang, G. Ji, Y. Gao, W. Fu, M. Irfan, L. Mu, Y. Zhang and A. Li, *J. Cleaner Prod.*, 2020, **264**, 121516.
106 J. C. Yuchen Liu, X. Zhu, F. Qian and S. Zhang, *RSC Adv.*, 2014, **4**, 63620–63626.
107 E. Cho, J. Kang, J. Moon, B. Um, C. Lee, S. Jeong and S. Park, *J. Environ. Chem. Eng.*, 2021, **9**, 106343.
108 Y. Yu, Q. Huang, J. Cui, K. Zhang, C. Tang and X. Peng, Springer, 2011, vol. 399, pp. 891–902.
109 K. Zoroufchi Benis, S. Minaei, J. Soltan and K. N. McPhedran, *Chem. Eng. Res. Des.*, 2022, **187**, 140–150.
110 F. M. Mpatani, A. A. Aryee, A. N. Kani, R. Han, Z. Li, E. Dovi and L. Qu, *J. Cleaner Prod.*, 2021, **308**, 127359.

111 A. A. Aryee, F. M. Mpatani, E. Dovi, Q. Li, J. Wang, R. Han, Z. Li and L. Qu, *J. Cleaner Prod.*, 2021, **329**, 129722.
112 C. Cheng, J. Zhang, C. Zhang, H. Liu and W. Liu, *Desalin. Water Treat.*, 2014, **52**, 5401–5412.
113 M. G. Lee and S. K. Kam, *Korean Chem. Eng. Res.*, 2018, **56**, 568–576.
114 A. A. Mohammed, T. J. Al-Musawi, S. L. Kareem, M. Zarrabi and A. M. Al-Ma'abreh, *Arabian J. Chem.*, 2019, **13**, 4629–4643.
115 H. R. Pouretedal and N. Sadegh, *J. Water Process. Eng.*, 2014, **1**, 64–73.
116 M. Xie, W. Chen, Z. Xu, S. Zheng and D. Zhu, *Environ. Pollut.*, 2014, **186**, 187–194.
117 L. Zhang, L. Tong, P. Zhu, P. Huang, Z. Tan, F. Qin, W. Shi, M. Wang, H. Nie, G. Yan and H. Huang, *Water Sci. Technol.*, 2018, **78**, 1336–1347.
118 C. Li, X. Zhu, H. He, Y. Fang, H. Dong, J. Lü, J. Li and Y. Li, *J. Mol. Liq.*, 2019, **274**, 353–361.
119 P. Liu, W. J. Liu, H. Jiang, J. J. Chen, W. W. Li and H. Q. Yu, *Bioresour. Technol.*, 2012, **121**, 235–240.
120 C. V. Gómez-Pacheco, J. Rivera-Utrilla, M. Sánchez-Polo and J. J. López-Peñalver, *J. Hazard. Mater.*, 2012, **217–218**, 76–84.
121 D. Huang, X. Wang, C. Zhang, G. Zeng, Z. Peng, J. Zhou, M. Cheng, R. Wang, Z. Hu and X. Qin, *Chemosphere*, 2017, **186**, 414–421.
122 Y. Chen, J. Shi, Q. Du, H. Zhang and Y. Cui, *RSC Adv.*, 2019, **9**, 14143–14153.
123 Y. Xiang, X. Yang, Z. Xu, W. Hu, Y. Zhou, Z. Wan, Y. Yang, Y. Wei, J. Yang and D. C. W. Tsang, *Sci. Total Environ.*, 2020, **709**, 136079.
124 D. Cheng, H. H. Ngo, W. Guo, S. W. Chang, D. D. Nguyen, X. Zhang, S. Varjani and Y. Liu, *Sci. Total Environ.*, 2020, **720**, 137662.
125 T. W. Tzeng, Y. T. Liu, Y. Deng, Y. C. Hsieh, C. C. Tan, S. L. Wang, S. T. Huang and Y. M. Tzou, *Int. J. Environ. Sci. Technol.*, 2016, **13**, 973–984.
126 N. Rattanachueskul, A. Saning, S. Kaowphong, N. Chumha and L. Chuenchom, *Bioresour. Technol.*, 2017, **226**, 164–172.
127 X. Zhu, Y. Liu, G. Luo, F. Qian, S. Zhang and J. Chen, *Environ. Sci. Technol.*, 2014, **48**, 5840–5848.
128 J. P. Simonin, *Chem. Eng. J.*, 2016, **300**, 254–263.
129 P. Saha, S. Chowdhury, S. Gupta and I. Kumar, *Chem. Eng. J.*, 2010, **165**, 874–882.
130 K. A. Guimarães Gusmão, L. V. Alves Gurgel, T. M. Sacramento Melo and L. F. Gil, *Dyes Pigm.*, 2012, **92**, 967–974.
131 B. Ohs, M. Krödel and M. Wessling, *Sep. Purif. Technol.*, 2018, **204**, 13–20.
132 M. Doğan, H. Abak and M. Alkan, *J. Hazard. Mater.*, 2009, **164**, 172–181.
133 H. Qiu, L. Lv, B. C. Pan, Q. J. Zhang, W. M. Zhang and Q. X. Zhang, *J. Zhejiang Univ., Sci., A*, 2009, **10**, 716–724.
134 J. Chen, X. Shi, Y. Zhan, X. Qiu, Y. Du and H. Deng, *Appl. Surf. Sci.*, 2017, **397**, 133–143.
135 D. H. K. Reddy, Y. Harinath, K. Seshaiah and A. V. R. Reddy, *Chem. Eng. J.*, 2010, **162**, 626–634.
136 K. Wang, H. Ren, Z. Wang, S. Ma, J. Wei, W. Ke and Y. Guo, *Nat. Resour. Res.*, 2021, **30**, 4597–4620.
137 R. Serna-Guerrero and A. Sayari, *Chem. Eng. J.*, 2010, **161**, 182–190.
138 M. A. Malana, R. B. Qureshi and M. N. Ashiq, *Chem. Eng. J.*, 2011, **172**, 721–727.
139 M. Benjelloun, Y. Miyah, G. Akdemir Evrendilek, F. Zerrouq and S. Lairini, *Arabian J. Chem.*, 2021, **14**, 103031.
140 J. A. Heimberg, K. J. Wahl, I. L. Singer and A. Erdemir, *Appl. Phys. Lett.*, 2001, **78**, 2449–2451.
141 W. Rudzinski and T. Panczyk, *J. Phys. Chem. B*, 2000, **104**, 9149–9162.
142 N. Y. Mezenner and A. Bensmaili, *Chem. Eng. J.*, 2009, **147**, 87–96.
143 S. S. Baral, N. Das, G. Roy Chaudhury and S. N. Das, *J. Hazard. Mater.*, 2009, **171**, 358–369.
144 S. M. Ahmed, M. R. Taha and O. M. E. Taha, *Nanotechnol. Environ. Eng.*, 2018, **3**(1), 4.
145 Y. dong Huang, *Appl. Surf. Sci.*, 2019, **469**, 564–565.
146 S. Afroze and T. K. Sen, *Water, Air, Soil Pollut.*, 2018, **229**, 225.
147 S. Chowdhury and P. Saha, *Chem. Eng. J.*, 2010, **164**, 168–177.
148 Z. Y. Yao, J. H. Qi and L. H. Wang, *J. Hazard. Mater.*, 2010, **174**, 137–143.
149 W. J. Weber and J. C. Morris, *J. Sanit. Eng. Div.*, 1963, **89**, 31–59.
150 C. Aharoni and M. Ungarish, *J. Chem. Soc., Faraday Trans. 1*, 1977, **73**, 456–464.
151 I. I. Laskar and Z. Hashisho, *Sep. Purif. Technol.*, 2020, **241**, 241.
152 K. L. Tan and B. H. Hameed, *J. Taiwan Inst. Chem. Eng.*, 2017, **74**, 25–48.
153 K. H. Chu, *Chem. Eng. J.*, 2020, **398**, 122513.
154 I. Langmuir, *J. Am. Chem. Soc.*, 1917, **39**, 1848–1906.
155 H. M. F. Freundlich, *J. Phys. Chem.*, 1906, **57**, 385–471.
156 G. S. Bohart and E. Q. Adams, *J. Am. Chem. Soc.*, 1920, **42**, 523–544.
157 S. Brunauer, P. H. Emmett and E. Teller, *J. Am. Chem. Soc.*, 1938, **60**, 309–319.
158 M. M. Dubinin, *Dokl. Akad. Nauk SSSR*, 1947, **55**, 327–329.
159 R. Saadi, Z. Saadi, R. Fazaeli and N. E. Fard, *Korean J. Chem. Eng.*, 2015, **32**, 787–799.
160 T. L. Hill, *Adv. Catal.*, 1952, **4**, 211–258.
161 A. R. Khan, R. Ataullah and A. Al-Haddad, *J. Colloid Interface Sci.*, 1997, **194**, 154–165.
162 R. A. Koble and T. E. Corrigan, *Ind. Eng. Chem.*, 1952, **44**, 383–387.
163 W. G. McMILLAN and E. TELLER, *J. Phys. Colloid Chem.*, 1951, **55**, 17–20.
164 A. L. Myers and J. M. Prausnitz, *AIChE J.*, 1965, **11**, 121–127.
165 O. Redlich and D. L. Peterson, *J. Phys. Chem.*, 1959, **63**, 1024.
166 R. Sips, *J. Chem. Phys.*, 1948, **16**, 490–495.
167 V. Tempkin and M. I. Pyzhev, *Acta Physicochim. URSS*, 1940, **12**, 327–356.
168 J. Toth, *Acta Chim. Acad. Sci. Hung.*, 1971, **69**, 311–317.

169 S. Das, A. Barui and A. Adak, *J. Water Process. Eng.*, 2020, **37**, 101497.
170 M. J. Ahmed and B. H. Hameed, *Ecotoxicol. Environ. Saf.*, 2018, **149**, 257–266.
171 M. Wahab, M. Zahoor, S. Muhammad Salman, A. W. Kamran, S. Naz, J. Burlakovs, A. Kallistova, N. Pimenov and I. Zekker, *Water*, 2021, **13**, 1969.
172 S. Y. Elovich and O. G. Larionov, *Bull. Acad. Sci. USSR Div. Chem. Sci.*, 1962, **11**, 198–203.
173 S. Kaur, S. Rani, R. K. Mahajan, M. Asif and V. K. Gupta, *J. Ind. Eng. Chem.*, 2015, **22**, 19–27.
174 V. J. Inglezakis, *Microporous Mesoporous Mater.*, 2007, **103**, 72–81.
175 G. Alberti, V. Amendola, M. Pesavento and R. Biesuz, *Coord. Chem. Rev.*, 2012, **256**, 28–45.
176 Q. Hu and Z. Zhang, *J. Mol. Liq.*, 2019, **277**, 646–648.
177 T. Shahnaz, V. Vishnu Priyan, S. Pandian and S. Narayanasamy, *Environ. Pollut.*, 2021, **268**, 115494.
178 O. S. Bello, K. A. Adegoke, A. A. Inyinbor and A. O. Dada, *Water Environ. Res.*, 2021, **93**, 2308–2328.
179 L. Largitte and R. Pasquier, *Chem. Eng. Res. Des.*, 2016, **109**, 495–504.
180 C. S. Patil, D. B. Gunjal, V. M. Naik, N. S. Harale, S. D. Jagadale, A. N. Kadam, P. S. Patil, G. B. Kolekar and A. H. Gore, *J. Cleaner Prod.*, 2019, **206**, 407–418.
181 I. Cabrita, B. Ruiz, A. S. Mestre, I. M. Fonseca, A. P. Carvalho and C. O. Ania, *Chem. Eng. J.*, 2010, **163**, 249–255.
182 H. A. Al-Yousef, B. M. Alotaibi, F. Aouaini, L. Sellaoui and A. Bonilla-Petriciolet, *J. Mol. Liq.*, 2021, **331**, 115697.
183 Y. Zhao, W. Li, J. Liu, K. Huang, C. Wu, H. Shao, H. Chen and X. Liu, *Chem. Eng. J.*, 2017, **326**, 745–755.
184 M. A. Chayid and M. J. Ahmed, *J. Environ. Chem. Eng.*, 2015, **3**, 1592–1601.
185 G. A. Haghighat, M. H. Saghi, I. Anastopoulos, A. Javid, A. Roudbari, S. S. Talebi, S. K. Ghadiri, D. A. Giannakoudakis and M. Shams, *J. Mol. Liq.*, 2020, **313**, 113523.
186 A. U. Rajapaksha, M. Vithanage, M. Ahmad, D. C. Seo, J. S. Cho, S. E. Lee, S. S. Lee and Y. S. Ok, *J. Hazard. Mater.*, 2015, **290**, 43–50.
187 A. C. Martins, O. Pezoti, A. L. Cazetta, K. C. Bedin, D. A. S. Yamazaki, G. F. G. Bandoch, T. Asefa, J. V. Visentainer and V. C. Almeida, *Chem. Eng. J.*, 2015, **260**, 291–299.
188 D. L. C. Rodrigues, F. M. Machado, A. G. Osório, C. F. de Azevedo, E. C. Lima, R. S. da Silva, D. R. Lima and F. M. Gonçalves, *Environ. Sci. Pollut. Res.*, 2020, **27**, 41394–41404.
189 E. Angulo, L. Bula, I. Mercado, A. Montaño and N. Cubillán, *Bioresour. Technol.*, 2018, **257**, 17–22.
190 S. bozorginia, J. Jaafari, K. Taghavi, S. D. Ashraf, E. Roohbakhsh and D. Naghipour, *Int. J. Environ. Anal. Chem.*, 2021, 1–15.
191 E. Azamateslamtalab, M. Madani, B. Ramavandi and R. Mohammadi, *Environ. Sci. Pollut. Res.*, 2020, **27**, 35792–35801.
192 N. Genç and E. C. Dogan, *Desalin. Water Treat.*, 2015, **53**, 785–793.
193 A. A. Kadam, B. Sharma, G. D. Saratale, R. G. Saratale, G. S. Ghodake, B. M. Mistry, S. K. Shinde, S. C. Jee and J. S. Sung, *Cellulose*, 2020, **27**, 3301–3318.
194 H. R. Pouretedal and N. Sadegh, *J. Water Process. Eng.*, 2014, **1**, 64–73.
195 M. Yuan, C. Li, B. Zhang, J. Wang, J. Zhu, J. Ji and Y. Ma, *Chemosphere*, 2021, **280**, 130877.
196 Y. Wang, W. Bin Jiao, J. T. Wang, G. F. Liu, H. L. Cao and J. Lü, *Bioresour. Technol.*, 2019, **277**, 128–135.
197 V. M. Nurchi, M. Crespo-Alonso, M. I. Pilo, N. Spano, G. Sanna and R. Toniolo, *Arabian J. Chem.*, 2019, **12**, 1141–1147.
198 Y. Jia, Q. Zong, M. Zhang, Z. M. Wang and L. H. Zhang, *Bull. Chin. Ceram. Soc.*, 2016, **35**, 815–818.
199 J. Ifthikar, X. Jiao, A. Ngambia, T. Wang, A. Khan, A. Jawad, Q. Xue, L. Liu and Z. Chen, *Bioresour. Technol.*, 2018, **262**, 22–31.
200 S. ye Wang, Y. kui Tang, C. Chen, J. tao Wu, Z. Huang, Y. yuan Mo, K. xuan Zhang and J. bo Chen, *Bioresour. Technol.*, 2015, **186**, 360–364.
201 G. Prasannamedha, P. S. Kumar, R. Mehala, T. J. Sharumitha and D. Surendhar, *J. Hazard. Mater.*, 2021, **407**, 124825.
202 K. Qiao, W. Tian, J. Bai, J. Dong, J. Zhao, X. Gong and S. Liu, *Ecotoxicol. Environ. Saf.*, 2018, **149**, 80–87.
203 X. He, M. Elkouz, M. Inyang, E. Dickenson and E. C. Wert, *J. Hazard. Mater.*, 2017, **326**, 101–109.
204 Y. Dai, N. Zhang, C. Xing, Q. Cui and Q. Sun, *Chemosphere*, 2019, **223**, 12–27.
205 E. Gagliano, M. Sgroi, P. P. Falciglia, F. G. A. Vagliasindi and P. Roccaro, *Water Res.*, 2020, **171**, 115381.
206 L. Cseri, M. Razali, P. Pogany and G. Szekely, *Green Chemistry: An Inclusive Approach*, Elsevier, 2018, pp. 513–553.
207 P. N. Omo-Okoro, A. P. Daso and J. O. Okonkwo, *Environ. Technol. Innovation*, 2018, **9**, 100–114.
208 Y. Shao, H. Zhang and Y. Yan, *Chem. Eng. J.*, 2013, **225**, 481–488.
209 E. Worch, *Adsorption Technology in Water Treatment: Fundamentals, Processes, and Modeling*, De Gruyter, 2021.